

1 **Novel populations of CD4⁺ T cells associated with vaccine efficacy**

2
3
4 **Authors:** Therese Woodring, MD¹; Colin N. Dewey, PhD²; Lucas Dos Santos Dias, PhD¹; Xin He, PhD¹;
5 Hannah E. Dobson¹; Marcel Wüthrich, PhD^{1*}; Bruce Klein, MD^{1,2,3*}

6
7 **Affiliations:** From the Departments of Pediatrics¹, Internal Medicine², Biostatistics and Medical
8 Informatics³, and Medical Microbiology and Immunology⁴ at the University of Wisconsin School of
9 Medicine and Public Health, University of Wisconsin-Madison, Madison WI.

10
11 **Address correspondence to:** Bruce Klein, MD, or Marcel Wüthrich, PhD, University of Wisconsin,
12 1550 Linden Dr., Madison WI 53706, at bsklein@wisc.edu

13
14 **Author contributions:** T.W. and C.D. contributed scRNAseq analysis; C.D. contributed to TCR and
15 gene velocity analysis; L.D., X.E., and H.D. contributed mouse and RT-PCR experimental data; T.W.
16 drafted the manuscript; M.W. and B.K. conceived project and oversaw intellectual content; and all
17 authors contributed to editing of manuscript.

18
19 ***These two authors contributed equally.**

20
21 **Competing interests:** The authors declare no competing interests.
22

23 **ABSTRACT**

24 Memory T cells underpin vaccine-induced immunity but are not yet fully understood. To distinguish
25 features of memory cells that confer protective immunity, we used single cell transcriptome analysis to
26 compare antigen-specific CD4⁺ T cells recalled to lungs of mice that received a protective or
27 nonprotective subunit vaccine followed by challenge with a fungal pathogen. We unexpectedly found
28 populations specific to protection that expressed a strong type I interferon response signature, whose
29 distinctive transcriptional signature appeared unconventionally dependent on IFN- γ receptor. We also
30 detected a unique population enriched in protection that highly expressed the gene for the natural killer
31 cell marker NKG7. Lastly, we detected differences in TCR gene use and in Th1- and Th17-skewed
32 responses after protective and nonprotective vaccine, respectively, reflecting heterogeneous *Ifn* γ - and
33 *Il17a*-expressing populations. Our findings highlight key features of transcriptionally diverse and
34 distinctive antigen-specific T cells associated with protective vaccine-induced immunity.

35 INTRODUCTION

36 Vaccines have saved millions of lives, eradicated fatal diseases, and proved essential to controlling
37 emerging infectious disease threats (Duclos et al., 2009; Galvani et al., 2021; Heaton, 2020). While
38 vaccines were initially developed without mechanistic understanding of immunity, they are now
39 recognized to require the response of antigen-specific T cells that produce cytokines to activate
40 phagocytes, induce antibody production in memory B cells, and persist long after the initial antigen
41 challenge. These memory T cells—including circulating effector memory T cells (T_{EM}), central memory
42 T cells (T_{CM}), and tissue-resident memory cells (T_{RM})—may be elicited by a variety of vaccine types and
43 confer variable protection based on the route of vaccination and magnitude of the initial T cell response
44 (Panagioti et al., 2018; Pollard and Bijker, 2021; Schenkel and Masopust, 2014). In contrast to circulating
45 antibodies, however, memory T cells can be difficult to isolate from the periphery and remain poorly
46 characterized. Given ongoing challenges in developing vaccines that induce cellular immunity against
47 some of the most important global pathogens, a better understanding of these T cells—and what
48 distinguishes protective from nonprotective vaccine-induced T cell responses—is a priority.

49
50 Single cell transcriptome analysis (scRNAseq) is one tool for characterizing memory T cells at the
51 site of pathogen encounter. Whereas traditional methods classify cells by expression of a small subset of
52 known markers, scRNAseq defines cell phenotypes agnostically, by gene expression profiles across the
53 entire transcriptome. Often, the approach validates known differences in cell types; however, it may also
54 expand or even challenge traditional frameworks for classifying complex populations. For instance,
55 scRNAseq analysis groups T cells from blood, lymphoid, and lung tissue by activation states distinct to
56 known $CD4^+$ and $CD8^+$ lineages, whereas effector T helper cells responding to various colonic pathogens
57 do not segregate into canonical Th1, Th2, and Th17 archetypes (Kiner et al., 2021; Szabo et al., 2019).

58
59 Sequencing-based methods also identify novel cell types (Stubington et al., 2017). One such cell,
60 observed in recent scRNAseq experiments, is the type I interferon-signature T cell (Andreatta et al., 2021;
61 Arazi et al., 2019; Gowthaman et al., 2019; Harsha Krovi et al., 2020; Kiner *et al.*, 2021; Seumois et al.,

62 2020; Singhanian et al., 2019; Szabo *et al.*, 2019; Tibbitt et al., 2019; Zemmour et al., 2018). These cells
63 (hereafter “Tis T cells”) are distinct for the striking upregulation of multiple genes that typically are
64 induced by type I interferons (IFN) and have well established roles in cellular responses to viral infection.
65 However, these Tis T cells have appeared across diverse immunological settings where type I interferon
66 would not be expected, such as dust mite allergy, *Alternaria* sensitization, and *Salmonella* and
67 *Citrobacter* infection (Gowthaman *et al.*, 2019; Kiner *et al.*, 2021; Tibbitt *et al.*, 2019). Their function
68 remains unknown.

69
70 Herein, we compare the transcriptional phenotypes of antigen-specific CD4⁺ T cells recalled to lungs
71 of mice challenged with lethal pulmonary fungal infection after they received a subunit vaccine that is
72 highly protective when given subcutaneously (SC), but not intranasally (IN). By using single cell
73 transcriptome analysis, we uncover populations of T cells previously unrecognized in the setting of
74 vaccine induced protective immunity. For example, we uncovered two T cell populations that express a
75 strong type I interferon response signature (Tis), unexpected in the context of antifungal immunity, but
76 consistent with descriptions of the novel Tis T cell phenotype recently reported in this journal. Unique to
77 our report, we observe increased abundance of Tis T cells only during a protective immune response,
78 together with the unconventional dependence of the Tis signature on IFN- γ receptor. We also highlight a
79 unique CD4⁺ T cell population enriched in protection that bears many NK cell markers including *Nkg7*, of
80 recent interest for its regulatory role in CD4⁺ T cell activation and pathogen control. Finally, while we
81 validate previously described Th1- and Th17-skewed responses after protective and nonprotective
82 vaccination, respectively, we uncover features of Th1 and Th17 responses that reflects a tension between
83 the widely accepted framework of conventional T helper cell archetypes (Th1, Th2, Th17) and the nuance
84 that can be detected by newer, hypothesis-free approaches to immune cell profiling

85 RESULTS

86 **scRNAseq analysis of antigen-specific memory CD4⁺ T cells from intranasally (IN) and**
87 **subcutaneously (SC) vaccinated, *Blastomyces*-challenged mice.** Mice were vaccinated either
88 intranasally (IN) or subcutaneously (SC) with *Blastomyces dermatitidis* endoglucanase-2 (BI-Eng2) six
89 weeks prior to pathogen challenge (Fig. 1a). As described previously, these routes of vaccine delivery
90 both induce substantial numbers of antigen-specific T cells but are associated with divergent outcomes in
91 response to lethal experimental challenge with *B. dermatitidis*. Mice vaccinated SC effectively control
92 lung fungal burden, whereas mice vaccinated IN do not (Dobson et al., 2020). For scRNAseq analysis,
93 tetramer-positive CD4⁺ T cells were FACS sorted and sequenced 3 days after the pulmonary challenge
94 with *B. dermatitidis* (Fig. 1b; Supplemental Fig. 1).

95
96 Integrated analysis of tetramer-positive cells from the IN and SC groups yielded 16 distinct cell
97 clusters numbered in order of decreasing size (Fig. 1c, Supplemental Table 1). **With exception of dividing**
98 **populations described below, clusters contained cells across all stages of the cell cycle and were not**
99 **affected by regression of cell cycle genes (Supplemental Fig. 1).** All cell clusters expressed *Cd3d* (CD3),
100 *Cd4* (CD4), and *Trac* (TCR α constant chain), consistent with the gating strategy to select for CD4⁺ T cells
101 (Fig. 2a). Most clusters also bore markers of tissue residence (T_{RM}) such as *Cd69* (CD69), the galectins
102 *Lgals1* and *Lgals3*, and *Vim* (vimentin) (Fig. 2b, Supplemental Fig. 2) (Szabo et al., 2019). Two
103 populations (clusters 9, 16) specifically expressed *Ccr7* and *Sell*, markers of resting naïve or T_{CM} T cells
104 that can be associated with lymphocyte transit to the site of infection (Fig. 2c) (Debes et al., 2005; Szabo
105 et al., 2019). These findings indicate the expected presence of CD4⁺ memory T cells specific to the
106 vaccine antigen with both tissue-resident and migratory phenotypes.

107
108 **Cluster identities.** Specific cluster identities were further interrogated by a combination of known marker
109 genes and cluster markers identified by scRNAseq differential expression analysis (Fig. 2d). The largest
110 populations bore conventional Th1 and Th17 cell signatures: high expression of *Ifng* (IFN γ) and Th1
111 transcription factor *Tbx21* (T-bet) (cluster 1); and high expression of *Il17a* (IL-17A), *Il17f* (IL-17F),

112 *Ccr6*, and Th17 transcription factor *Rorc* (ROR γ t) (cluster 2). Interestingly, these clusters adjoined a
113 spectrum of 5 additional populations also expressing Th1 genes, Th17 genes, or both (clusters 3-7). In
114 addition to their cytokine phenotype, these clusters were distinguished by expression of genes less
115 familiar to the classic Th framework, including: *Ctsw* and *Ctsd* (cathepsins W and D; cluster 4); *Vps37b*
116 (vacuolar protein sorting 37B) and *Ramp3* (receptor activity modifying protein 3) (cluster 6) (Miragaia et
117 al., 2019); co-stimulatory signaling genes *Tnfrsf4* (OX40/CD134) and *Tnfrsf9* (4-1BBL/CD137) (cluster
118 7); *Ramp1* (receptor activity modifying protein 1; cluster 5); and activator protein subunit genes *Jun* and
119 *Fos* (cluster 3).

120
121 An unexpected and remarkable finding is that two populations (clusters 8, 13) expressed high levels
122 of type I interferon response genes (*Stat1*, *Isg15*, *Ifi206*, *Ifit3*, *Mx1*). Although the type I interferon
123 response is classically understood as an antiviral program, this type I interferon signature (Tis) has been
124 described elsewhere outside of an antiviral immune context in CD4⁺ T helper cells, Tregs, and thymic
125 invariant natural killer T (iNKT) cells (Andreatta et al., 2021; Arazi et al., 2019; Gowthaman et al., 2019;
126 Harsha Krovi et al., 2020; Kiner et al., 2021; Seumois et al., 2020; Singhania et al., 2019; Szabo et al.,
127 2019; Tibbitt et al., 2019; Zemmour et al., 2020). Here, we adopt the term Tis T cells to describe these
128 distinct populations. We also observed a population (cluster 12) notable for very high expression of
129 chemokine *Ccl5* (CCL5) and multiple NK-cell markers including *Nkg7* (natural killer granule protein 7),
130 *Klrkl1* (CD94), and *Klrblc* (CD161). Since this cluster also expressed Th1 genes (*Ifng*, *Tbx21*) at a level
131 comparable to a conventional Th1 phenotype (cluster 1), we provisionally termed this cluster NK-like
132 Th1 cells.

133
134 The remaining populations included Tregs (*Foxp3*, *Ikzf2*; cluster 15), two populations of dividing
135 cells (*Cdk1*, *Mki67*, *Tuba1b*, *Stmn1*; clusters 14, 10), and naïve/T_{CM} cells (*Ccr7*, *Sell*; cluster 9) (Szabo et
136 al., 2019). We also saw a population of transcriptionally less active cells (cluster 11) that expressed
137 markers for prolonged survival (*Bcl2*, *Cdk6*), suggesting quiescent cells distinct from the resting
138 naïve/T_{CM} population expressing *Ccr7* and *Sell* (Supplemental Fig. 2) (Cheng et al., 2004). Lastly, we

139 observed a very small population of cells bearing myeloid markers (*H2-Ab1*, *ApoE*, *Lyz2*; cluster 16).
140 Since this smallest group of cells still expressed CD4⁺ T cell markers and did not exhibit increased reads
141 suggestive of myeloid cell-T cell doublets (Supplemental Fig. 2), we tentatively labeled them myeloid-
142 like T (MyT) cells, adopting the term for a population of $\alpha\beta$ T cells that acquire myeloid markers
143 peripherally and have been validated elsewhere with flow cytometry and RNAseq (Kiner *et al.*, 2021).
144 Our ability to validate this novel cell type, however, was limited by the small number of cells for analysis
145 (N=44, 0.2% all cells).

146
147 **Differential abundance and gene expression between cells from IN and SC vaccinated mice.** The
148 relative abundance of many clusters differed between the IN and SC groups (Fig. 3a,b; Supplemental
149 Table 1, Supplemental Fig. 1). IN populations with increased relative abundance included *Il17a*-
150 producing clusters (clusters 2, 6, 7), naïve/ T_{CM} cells (cluster 9), one population of dividing cells (cluster
151 14), and Tregs (cluster 15). By contrast, SC populations with increased relative abundance included *Ifng*-
152 expressing clusters (clusters 1, 4), Tis T cells (clusters 8, 13), and NK-like Th1 cells (cluster 12).
153 Unsurprisingly, the shift in relative abundance was associated with differential gene expression across all
154 antigen-specific cells in the IN group compared to SC group (Fig. 3c; Supplemental Table 2). Average
155 *Il17a* expression was higher for the IN group, consistent with a Th17-skewed response to pathogen
156 challenge seen previously with this route of vaccination, as was expression of other intercellular signaling
157 genes including *Ccr6* (CCR6) and *Cxcr4* (CXCR4) (Dobson *et al.*, 2020). By contrast, the SC group
158 showed higher average expression of *Ifng*, macrophage- and granulocyte/macrophage- stimulating genes
159 *Csf1* (M-CSF) and *Csf2* (GM-CSF), the chemokine *Ccl5* (CCL5, aka RANTES), and chemokine receptor
160 *Cxcr6* (CXCR6). This skewed Th17 response in the unprotected IN group was unexpected, since Th17
161 response is generally believed to promote protection against fungi at mucosal surfaces (Huppler *et al.*,
162 2012).

163
164 Other salient differences included increased expression in the SC group of type I interferon response
165 genes and NK cell markers, as would be expected with increased abundance of Tis T and NK-like Th1

166 cells. In the IN group, we also observed increased expression of some activation-related genes such as Jun
167 and Fos family genes (*Jun*, *Junb*, *Fos*, *Fosl2*) and activation-induced immune checkpoint gene *Ctla4*
168 (CTLA-4) (Kiner *et al.*, 2021). Since high activation genes did not universally segregate to the IN group,
169 nor low activation genes to the SC group, this data suggests complexity beyond the hypothesis that one
170 vaccine route might prime a more activated CD4⁺ T cell phenotype than the other route during pathogen
171 challenge. Nevertheless, our data showed a trend towards increased expression of some exhaustion
172 markers such as *Ikzf2* (Helios), *Lag3* (Lymphocyte activation gene 3), and *Pdcd1* (Programmed cell death
173 1 [Pd1]) (Fig. 3c). While this difference did not correspond to marked differences between the IN and SC
174 groups in the relative abundance of proliferating cells (Fig. 3b), we did observe increased expression of
175 activation-induced immune checkpoint gene *Ctla4* in the IN group, which was not exclusively explained
176 by the increased abundance of Tregs, but rather appeared to reflect specific downregulation of this critical
177 checkpoint gene in non-Treg clusters in the SC group (Fig. 3d, e). This data may suggest greater
178 activation-induced exhaustion in the IN group, or perhaps escape from this negative feedback mechanism
179 in the protective vaccine-induced immune response.

180
181 **Analysis of Th1 and Th17 phenotypes.** We next analyzed characteristic Th1 and Th17 cytokine gene
182 expression at the single cell level. Interestingly, the Th17 cytokine phenotype in the IN group reflected
183 not only the relative expansion of populations characterized by *Il17a* expression regardless of vaccination
184 route (e.g. cluster 2), but also from an increased *Il17a* expression within populations that would otherwise
185 express *Ifng* in mice vaccinated SC (e.g. cluster 3) (Fig. 3f). Similarly, the Th1 cytokine phenotype in the
186 SC group appeared associated with increased abundance of populations restricted to *Ifng* expression (e.g.
187 clusters 1, 4) as well as a switch from *Il17a* to *Ifng* dominance in other Th1/Th17 populations. The
188 distribution of Th1 and Th17 transcription factors *Tbx21* (Tbet) and *Rorc* (ROR γ t) mirrored the patterns
189 seen in downstream cytokine expression (Supplemental Fig. 2). This fluidity of the dominant cytokine
190 phenotypes in Th1/Th17 cells complicates assignments of strict Th archetypes and may align with
191 evolving notions of Th cell cytokine plasticity, for instance in Th17 cells described elsewhere (Zhu and

192 Paul, 2010). Alternatively, this result may indicate dual cytokine production among cells from each
193 vaccine group. There were stable small fractions of cells producing both cytokines simultaneously (Fig.
194 3f), though the limited sequencing depth for each cell in scRNAseq makes it challenging to differentiate
195 whether these subpopulations are a true minority or simply undersampled.

196
197 **TCR gene usage.** We explored whether cytokine phenotypes reflected the presence of a few expanded,
198 highly active T cell clones, or a broader diversity of T cells responding to pathogen challenge. Using
199 TRUST4, an algorithm that infers TCR clonotypes using focused reconstruction of variable TCR gene
200 regions (Song et al., 2021), we recovered sufficient TCR sequence data from all 16 clusters to assign
201 clonotypes by α , β , or combined $\alpha\beta$ TCR sequences to 2,421 and 2,619 T cells in the IN and SC samples,
202 respectively (Supplemental Fig. 3). Especially for α and $\alpha\beta$ chains, we observed that clonotypes tended to
203 be skewed in distribution between the IN and SC groups, with individual clonotypes occurring
204 predominantly in either one or the other group (Fig. 4a). The IN group showed dominance of relatively
205 few clonotypes, while the SC group exhibited more even representation of clonotypes comprising at least
206 2% of either sample (Fig. 4b, Supplemental Fig. 3). In both groups, the most frequent clonotypes were
207 most abundant in the largest clusters expressing high levels of Th1 and Th17 cytokines (e.g., clusters 1-7;
208 Fig. 4c, Supplemental Fig. 3). Thus, the size of these clusters appeared to reflect expanded, active T cell
209 clones, with many TCR sequences unique to either the IN or SC group.

210
211 **Special populations in nonprotective immune response: Tregs.** We noted the higher relative
212 abundance of *Foxp3*-expressing Tregs in the nonprotective IN vaccine-induced immune response (Fig.
213 5a), consistent with prior experimental data in this model (Dobson *et al.*, 2020). Since mucosal antigen
214 exposure can induce systemic immune tolerance, we wondered whether these Tregs might be impairing
215 pathogen clearance by actively suppressing antifungal immunity (Rezende and Weiner, 2017). Tregs in
216 the IN group, however, did not express high levels of tolerogenic cytokine genes such as *Tgfb1*
217 (transforming growth factor β), *Il10* (interleukin-10), or *Il4* (interleukin-4) (Fig. 5b). Nor did we observe
218 increased expression of markers of T cell anergy (e.g. *Rnf128* [GRAIL]) to suggest other mechanisms of

219 tolerance in cells of the IN group (Supplemental Fig. 4). Indeed, other observed features of the response
220 to pathogen challenge in the IN group, including prominent *Il17a* expression, appeared more consistent
221 with pro-inflammatory response to a lethal pathogen than with microbial tolerance.

222
223 **Special populations in protective immune response: NK-like Th1 cells.** We explored whether
224 populations specific to the SC group might explain the distinctive efficacy of this vaccine immune
225 response. One such population was the NK-like Th1 cells (cluster 12), for which a gene set enrichment
226 analysis of its expression profile relative to cells from all other clusters resulted in the NK cell type as the
227 most significantly enriched mouse cell type signature (adjusted p-value < 3×10^{-9}). This cluster was
228 distinct for high levels of NK markers such as *Nkg7* (natural killer granule protein 7), *Klrk1c* (CD161),
229 and *Klrk1* (CD94) (Fig. 5c). Among these markers, *Nkg7* raised particular interest due to an emerging
230 role for inducible *Nkg7* in CD4⁺ T cells, where it appears to be associated with IFN γ expression and
231 promote parasite control in a model of *Leishmania donovani* infection (Ng et al., 2020). Indeed, we
232 observed increased *Nkg7* expression in those populations enriched in the SC group's *Ifng*-polarized
233 immune response, including in the highest *Ifng*-expressing populations (clusters 1, 4, 3), Tis T cells
234 (clusters 13, 8), and NK-like Th1 cells (Fig. 5d). These NK-like Th1 cells were also notable for specific
235 expression of the gene *Ccl5* (CCL5 or RANTES), a pleiotropic chemokine that attracts effector and
236 memory cells to the site of infection and is unique among CC-type chemokines for its role in the later
237 stages of response to infection (Fig. 5e) (Ortiz et al., 1996). Notably, while NK markers such as granzyme
238 (*Gzmb*) and perforin (*Prfl*) are associated with cytotoxic function, our NK-like Th1 cells did not express
239 markers of cytotoxic CD4⁺ T cells, a recently described population that appears capable of inducing
240 apoptosis of target cells in an MHC class II-restricted manner (Supplemental Fig. 4) (Takeuchi and Saito,
241 2017).

242
243 Based on NK markers, we considered whether these cells might be NKT cells, an innate-like T cell
244 population that expresses $\alpha\beta$ TCR and combines NK cell reactivity with some of the antigen-specificity of
245 T cells (Godfrey et al., 2004). Indeed, cluster 12 cells expressed many of the genes up- and down-

246 regulated in Th1-like NKT cells (NKT1) by scRNAseq profiling (Fig. 5f) (Engel et al., 2016).
247 Importantly, however, these cells lacked expression of the gene for PZLF (*Zbtb16*), a transcription factor
248 marker for most innate and innate-like T cell populations including NKT cells (Supplemental Fig. 4)
249 (Mao et al., 2017). Moreover, the TCR of NKT cells classically binds Cd1d, an MHC class I-type
250 receptor that presents lipid antigen, and would not be expected to bind the MHC class II tetramer and
251 peptide antigen used to sort our B1-Eng2-specific T cells. While some have reported NKT cells in CD1d-
252 deficient mice—including CCL5 producers as seen here—others insist on CD1d-restriction as an essential
253 feature for the term NKT to remain meaningful (Eberl et al., 1999; Farr et al., 2014; Giroux and Denis,
254 2005; Godfrey *et al.*, 2004). We opted for the term NK-like Th1 cells, emphasizing core Th1 features
255 with additional NK marker expression. In either case, the appearance of this NK-like Th1 phenotype and
256 the accompanying chemokine activity were salient, previously undescribed features of vaccine-induced
257 protective immunity to fungi.

258
259 **Special populations in the protective immune response: Tis T cells.** Tis (type I interferon signature) T
260 cells (clusters 8, 13) were another cell phenotype associated with the protective immune response.
261 Especially in the SC group, these cells comprised a meaningful portion of our tetramer positive T cells,
262 representing 12.6% and 4.2% of all cells in the SC and IN vaccine groups, respectively (Fig. 6a). These
263 populations showed a transcriptional signature dominated by several type I interferon-responsive genes
264 (*Ifitm3*, *Ifi204*, *Isg15*, *Isg20*, *Mx1*, *Rsad2*, *Oas3*, etc.) (Fig. 6b). This signature included genes upstream in
265 type I interferon signal transduction, such as *Stat1* (Stat1) and *Stat2* (Stat2), and those associated with
266 distal interferon response functions such as global suppression of translation (*e.g.* *Eif2ak2* [EIF2 α kinase
267 2]), processing of cytosolic DNA and RNA (*e.g.* *Ddx58* [RIG-I], *Zbp1* [Z-DNA binding protein 1], and
268 *Samhd1* [SAM and HD domain 1]), and protection from viral infections including influenza and SARS-
269 CoV-2 (*Ifitm3* [interferon-induced transmembrane protein 3]) (Fig. 6c, Supplemental Table 3) (Everitt et
270 al., 2012; Prelli Bozzo et al., 2021). Other Tis T cell genes coding for transmembrane proteins (*Rtp4*, *Bst2*

271 [tetherin/CD317]) and nuclear body proteins (*Pml*, *Sp100*) were noteworthy as potential cell surface or
272 microstructural markers.

273
274 **Tis T cell heterogeneity.** Tis T cells separated into 2 clusters that shared a common strong type I
275 interferon signature (Fig. 6c). However, one Tis T cell population (cluster 8) distinctly expressed more
276 *Bhlhe40* (basic helix-loop-helix family member e40), a key transcription factor that characterizes a highly
277 pro-inflammatory phenotype in CD4⁺ memory T cells (Fig. 6d, Supplemental Table 4) (Emming et al.,
278 2020). This same Tis T cell cluster also expressed higher levels of NF-κB inhibitors *Nfkbia* (IκBa),
279 *Nfkbid* (IκBNS), and *Nfkbiz* (IκBζ) (Emming et al., 2020), activator protein 1 (AP-1) subunit genes *Junb*
280 (*Junb*) and *Fosl2* (*Fra2*), histone and histone modulating genes (e.g. *H3f3b* [H3.3 histone B], *Kdm6b*
281 [lysine demethylase 6B]), and *Zc3h12a* (MCPIP1 or regnase-1) (Garg et al., 2015; Matsushita et al.,
282 2009). Remarkably, many of these same markers have appeared recently in another scRNAseq analysis of
283 CD4⁺ T cell heterogeneity, in which transcriptional diversity was driven primarily by activation state
284 rather than by conventional Th archetype as might have been expected (Kiner, 2019; Kiner et al., 2021).
285 In that analysis, activation-related genes (e.g. *Bhlhe40*, *Jund*, *Dusp1*, *Btg1*, *Odc1*, *Vps37b*) comprised the
286 first principal component (PC1) driving transcriptional diversity in CD4⁺ T cells following a variety of
287 enteric infections (Kiner, 2019). In querying our data for these PC1 genes, we saw that differing
288 expression not only separated our Tis T cell populations, but also organized non-Tis T cells into two
289 rough superclusters, in which Th1/Th17 clusters 4 and 5 grouped with cluster 13 Tis T cells apart from
290 surrounding Tis and non-Tis T cells (e.g. *Bhlhe40*, *Nfkbia*; Fig. 6e). This finding emphasized the
291 importance of activation state as an organizing principle for CD4⁺ T cell heterogeneity, including within
292 Tis T cells.

293
294 We considered whether the separation of Tis T cells into two populations (clusters 8 and 13) might
295 reflect a sequence of cell differentiation, in which one phenotype might be a precursor to the other. These
296 transitional patterns can be explored in scRNAseq with RNA velocity analysis. The ratio of unspliced and
297 spliced reads mapping to a given gene is compared to expected steady state kinetics to make a prediction

298 about an increase in transcription rate (with the resulting increase in unspliced mRNA) or vice versa (La
299 Manno et al., 2018). In our Tis T cells, however, we did not observe any genes characterizing the
300 expression profile of one cluster among the genes with most significantly different velocity in the other
301 (Supplemental Table 5). This finding suggests that one population is not a precursor of the other
302 population.

303
304 **Validation of Tis T cell phenotype.** We validated the presence of the Tis T cell phenotype by
305 quantitative RT-PCR in vaccinated mice after *Blastomyces* challenge. Consistent with scRNAseq data, we
306 detected a transcriptional signal for multiple Tis T cell marker genes (*Ifi204*, *Mx1*, *Pml*, *Slfn5*, *Ifit1*,
307 *Ifitm3*) present among tetramer⁺ antigen-specific CD44⁺ cells, but not among control (CD44⁻) cells, in
308 both the lung and spleen after pulmonary pathogen challenge (Fig. 7a, Supplemental Fig. 5). This
309 difference in expression was distinct from the upregulation of interferon response genes in both antigen-
310 specific and control cells following exposure to soluble type I interferon (IFN α), though the relative
311 enrichment of several Tis T cell transcripts in antigen-specific cells relative to control cells was still
312 detectable in this experiment. As expected, relative expression of Tis T cell markers *Ifi204* and *Ifitm3* was
313 increased in tetramer-positive T cells from SC vaccinated animals compared to those from the IN group
314 (Fig. 7b), conforming to results from our scRNAseq analysis (Fig. 3b).

315
316 **IFN γ R-dependence of Tis T cell signal.** We sought to understand upstream signaling for the Tis T cell
317 signature. Remarkably, despite an increased and highly specific type I interferon gene signature, our Tis T
318 cell populations did not express the type I interferon receptor genes *Ifnar1* (IFNAR1) and *Ifnar2*
319 (IFNAR2) (Fig. 7c) (Tibbitt et al., 2019). Other investigators studying *T. gondii*-infected mice have
320 described a strong type I IFN transcription module dependent on the presence of IFN γ R, another type II
321 cytokine receptor (Singhania et al., 2019). We hypothesized that this transcription module might reflect
322 the presence of Tis T cells and tested whether our Tis T cell signature may similarly depend on IFN γ R.
323 To explore this idea, we vaccinated IFN γ R^{-/-} (IFN γ R KO) mice SC. We found that, after pulmonary
324 challenge, the presence of signature transcripts for Tis T cells was diminished in tetramer⁺ antigen-

325 specific T cells, but not in CD44⁺ control cells (Fig. 7d). Thus, the emergence of Tis T cells requires
326 IFN γ R signaling. In contrast to the Tis T cell transcripts, the relative expression of *Il17a* was increased in
327 IFN γ R KO mice, suggesting a compensatory effect in the dynamic balance between Th1 and Th17
328 cytokine environments. Despite this potential compensation, IFN γ R KO did not acquire resistance after
329 SC vaccination. After pulmonary challenge, the lungs of these mice were grossly abnormal. They were
330 more swollen than the lungs of corresponding wild-type mice and with nodules and micro-abscesses
331 stippling the pleural surface. This increased inflammation was accompanied by increased percentages of
332 CD4⁺ T cells and tetramer-positive cells in the lungs of the IFN γ R KO mice compared to wild type mice
333 (Supplemental Fig. 5d)

334
335 Intriguingly, while scRNAseq data did show that Tis T cells express IFN γ R α -chain gene (*Ifngr1*),
336 these cells did not express the IFN γ R β -chain gene (*Ifngr2*) presumed to confer IFN γ responsiveness to T
337 cells (Fig. 7e) (Bach et al., 1997; Bach et al., 1995). Moreover, soluble IFN γ did not elicit any
338 upregulation of the Tis T cell signature genes in tetramer positive cells in our RT-PCR experiments
339 (Supplemental Fig. 5). Together, this data suggests the dependence of the Tis T cell signature on IFN γ R,
340 apparently by a mechanism distinct from classic IFN γ -IFN γ R receptor signaling.

341

342

343 **DISCUSSION**

344 Antigen-specific T cells are essential for vaccine-induced immunological memory and effective pathogen
345 control. Our work demonstrates key differences in the phenotypic profiles of antigen-specific CD4⁺ T
346 cells present at the site of pathogen challenge in a protective and nonprotective vaccine model. Our study
347 yields some distinctly surprising results in addition to expected findings. We observe unique cell
348 populations, including two with high expression of type I interferon signature genes and one highly
349 expressing *Ccl5*, that are associated specifically with protective vaccine-induced immunity. We also
350 redemonstrate essential differences in Th1- and Th17-skewing of protective and nonprotective vaccine-
351 induced responses, reflecting the activity of conventional appearing, clonally dominant Th1 and Th17
352 cells together with a spectrum of more phenotypically heterogeneous *Ifng*- and *Il17a*-expressing
353 populations.

354 We uncovered a Tis T cell phenotype enriched among antigen-specific cells that confer vaccine-
355 induced immunity. We did not expect to see type I interferon signaling in the context of vaccine-primed
356 responses to *B. dermatitidis*, a fungal pathogen traditionally understood to elicit Th1- and Th17-related
357 cytokines such as IFN- γ , TNF- α , IL-17, and IL-6 (Merkhofer et al., 2019; Speakman et al., 2020). Others
358 have recently observed Tis T cells in settings outside of viral infection (Andreatta et al., 2021; Arazi et
359 al., 2019; Gowthaman et al., 2019; Harsha Krovi et al., 2020; Kiner et al., 2021; Seumois et al., 2020;
360 Singhania et al., 2019; Szabo et al., 2019; Tibbitt et al., 2019; Zemmour et al., 2020). However, our
361 findings—validated by RT-qPCR—add new insight to this enigmatic, recently described population of T
362 cells. In our model, Tis T cells were associated with a protective, vaccine-induced immune response. We
363 also observed phenotypic heterogeneity underlying the Tis T cell signature that has not been previously
364 described, including divergent expression of the pro-inflammatory transcription factor *Bhlhe40* and other
365 activation-related genes that appear to be an organizing framework for CD4⁺ T cells across microbially
366 diverse infectious challenges (Emming et al., 2020; Kiner et al., 2021). The loss of the Tis T cell
367 signature in IFN γ R KO mice is another remarkable feature that merits future study. **We wonder whether**

369 the IFN γ R α -chain expressed nonspecifically in Tis T cells could bind another unidentified cytokine
370 receptor chain required for a novel type I IFN signature response, analogous to the combinatorial
371 plasticity seen in other cytokine signaling mechanisms (Morris et al., 2018). Alternatively, the loss of
372 IFN γ R could indirectly mute the Tis T cell response, e.g. through decreased T cell activation in IFN γ R
373 KO mice overall. These hypotheses and other features of Tis T cell biology, such as the possible
374 antagonism of Tis T cells by Th17 cells within the IN group, are exciting avenues for future functional
375 studies.

376 Our findings highlight the difficulties of classifying populations in scRNAseq that share features with
377 multiple conventionally defined cell types, which are often described by only a few markers. In our data,
378 NK-like Th1 cells make up one such population that resists straightforward identification based on
379 overlapping features with Th1, NK, and NKT cells. Nonetheless, this ambiguity will be important to
380 pursue. This population is a distinct feature of a protective vaccine-induced immune response in our
381 model and the sole source of *Ccl5* expression. CCL5 is known to be unique among CC chemokines as a
382 late-appearing signal, expressed three to five days after T cell activation, with a role in attracting effector
383 T cells and new memory T cells to the site of infection (Ortiz *et al.*, 1996; Seo et al., 2020). The high
384 expression of *Ccl5* three days after pathogen challenge in only the SC vaccine group might reflect a
385 mechanism of improved pathogen clearance by early cytokine production and effector cell recruitment
386 following protective vaccination. These cells also highly express *Nkg7*, a feature shared with other *Ifng*-
387 expressing populations in the SC vaccinated group. The potential association between *Nkg7* expression
388 and IFN γ activity aligns with new data linking *Nkg7* and CD4⁺ T cell activation and suggests a role for
389 this molecule in regulating key effector cytokines from CD4⁺ T cells in a protective vaccine-induced
390 immune response (Ng *et al.*, 2020).

391 Lastly, our analysis confirms the core distinction between IFN γ - and IL-17-skewed responses in
392 protective and nonprotective vaccine-induced immune responses, respectively (Dobson *et al.*, 2020).
393 Notably, the highest cytokine producing, clonally dominant Th1 and Th17 cells that express archetypical
394

395 Th markers lie at the extremes of a spectrum of phenotypes that differ by expression of genes that are
396 distinctly unfamiliar to a classic Th paradigm. For instance, among the 29 immune cell types of the
397 Monaco dataset shared in the Human Protein Atlas, the cluster 7 marker *Rgs16* appears more specific to B
398 cells than either Th1 or Th17 cells, and cluster 3 marker *Dnajb1* is similarly expressed in Th1, Th2, and
399 Th17 cells (Monaco et al., 2019; The Human Protein Atlas, 2019). This reflects a tension between the
400 widely accepted framework of conventional T helper cell archetypes (Th1, Th2, Th17) and the nuance
401 that can be detected by newer, hypothesis-free approaches to immune cell profiling. More work remains
402 to discern whether this heterogeneity is functionally meaningful—and if so, how it should be integrated
403 into an organizing principle that remains useful for understanding immune cell ontogeny. Of note, these
404 *Ifng*- and *Il17a*-expressing cell populations also appear to comprise largely non-overlapping TCR
405 clonotypes, which might reflect either the stochastic effects of random V(D)J recombination prior to TCR
406 selection by vaccination and pathogen challenge, some more active enrichment of specific TCR
407 sequences within the protective immune response, or a combination of both.

408
409 Overall, our high-resolution single cell analysis of antigen-specific T cells in pathogen challenge
410 provides insight into multiple dimensions of vaccine-related T cell biology. A general limitation of
411 scRNAseq data is depth of sequencing, which comes at the cost of sequencing large numbers of cells
412 (Zhang et al., 2020). More reads (*e.g.* greater depth) significantly reduces inaccuracy in estimating the
413 true transcriptional state of a cell, but sequencing of more cells enables a broader view of the biological
414 variability in the cell population. Consequently, we recognize that the absence of certain sequences does
415 not exclude low level expression that was undetectable in our analysis. Other limitations inherent to study
416 design include the lack of transcriptional data for antigen-nonspecific cells and of functional data for
417 populations identified by scRNAseq. While our study uncovered correlations between novel populations
418 of CD4 T cells and resistance, one should not assume causal relationships from the observed associations
419 between cell phenotypes (*e.g.* Tis T cells, NK-like Th1 cells) and biological outcomes such as improved
420 pathogen control following SC vaccination. Future studies are required to discern whether Tis T cells,

421 CCL5, or NKG7 are required for protective vaccine-induced immunity or are simply markers of this
422 response that is driven by other cellular events. Our analysis of TCR sequences is also limited by use of
423 conventional 3' library preparation, which provides less coverage of hypervariable regions clustered
424 towards the 5' end and may be reason for choosing 5' chemistry for more robust TCR analyses and
425 clonotype tracking in the future. Nonetheless, our work describes novel characteristics of vaccine-induced
426 T cells in protective immunity, including populations that could serve as correlates of efficacy in vaccine
427 design, and adds to the ongoing, exciting scientific pursuit of T cell diversity.

428 **METHODS**

429 **Mice.** *C57BL/6* mice from Jackson Laboratory were bred at our facility and cared for per guidelines from
430 the University of Wisconsin Animal Care Committee, who approved all aspects of this work. Mice were
431 7-8 weeks old at the start of experiments. Mice were vaccinated intranasally (IN) or subcutaneously (SC)
432 with 10 µg of BI-Eng2 in glucan chitin particles (CGP) a total of three times, two weeks apart. Two
433 weeks after the final vaccination, mice were challenged intratracheally with 2×10^4 *Blastomyces*
434 *dermatitidis* (*Bd*, ATCC strain 26199) and analyzed at day 3 post-infection.

435
436 **Flow cytometry.** We harvested cells from a total of 24 mice: 10 vaccinated SC and 14 vaccinated IN.
437 Cells were prepared from harvested lungs as described previously and pooled for each group. (Dobson *et*
438 *al.*, 2020) Briefly, lungs were harvested from challenged animals and dissociated in Miltenyi MACS
439 tubes (Miltenyi Inc., Germany) and digested with collagenase (1 mg/mL) and DNase (1 µg/mL) for
440 25 min at 37 °C. Digested lungs were resuspended in 5 mL of 40% percoll, and 3 mL of 66% percoll was
441 underlaid (GE healthcare 17-0891-01). Samples were spun for 20 min at 2000 rpm at room temperature.
442 Lymphocytes were then harvested from the buffy coat layer and resuspended in complete RPMI (10%
443 FBS, 1% penicillin and streptomycin). The cells were spun down (1500 rpm/5 minutes at room
444 temperature) and stained with LIVE/DEAD™ Fixable Near-IR Dead Cell Stain Kit (Invitrogen) and Fc
445 Block (BD) for 10 min at room temperature. Then the cells were stained with BI-Eng2 tetramer (MHC
446 class II tetramer-PE, NIH) for 1 hour at room temperature, and 30 minutes at 4°C with the following
447 surface antibodies: CD8 PerCP-Cy5.5 (clone 53-6.7, Biolegend, cat#100734), CD44 BV650 (clone IM7,
448 Biolegend, cat#103049), CD11b APC (clone M1/70, Biolegend, cat#101212), CD11c APC (clone N418,
449 Biolegend, cat#117310), NK1.1 APC (clone PK136, Biolegend, cat#108710), B220 APC (clone RA3-
450 62B, Biolegend, cat#103212), CD4 BUV737 (clone RM4-5, BD, cat#565246), and CD90.2 BV421
451 (clone 30-H12, Biolegend, cat#105341). All panels included a dump channel to decrease background in
452 CD4+ T cells (Dump: CD11b, CD11c, NK1.1, and B220). The cells were sorted using the cell sorting
453 flow cytometer FACS Aria (BD). Following fluorescent labeling, cells from 10-15 animals from each

454 vaccine (SC or IN) group were combined into one tube each for cell sorting. Tetramer⁺ cells were sorted
455 into microcentrifuge tubes containing RPMI media on a FACs Aria using a 130 micron nozzle. The sorted
456 cells (Live, Dump⁻CD90.2⁺CD4⁺CD44⁺Tetramer⁺) were collected directly into 1.5 ml microtubes and
457 provided to the UW-Madison Biotechnology Center for 10x Genomics Single Cell RNA sequencing.

458
459 **Single-cell RNA-seq libraries.** Sorted tetramer⁺ cells were counted on a Countless II cell counter with
460 0.4% trypan blue and concentrated to 300-400 cells/ml (total volume of 43.3 ml) and reverse transcribed.
461 The libraries were generated with the 3' kit version 3.1 chemistry (10x Genomics) and sequenced on the
462 MiSeq system and the NovaSeq 6000.

463
464 **Single-cell RNA-seq data analysis.** Single cell RNAseq data was initially processed by the UW
465 Bioinformatics Resource Center. Experiment data was demultiplexed using the Cell Ranger Single Cell
466 Software Suite, mkfastq command wrapped around Illumina's bcl2fastq (v2.20.0.422). The MiSeq
467 balancing run was quality controlled using calculations based on UMI-tools (Smith et al., 2017). Samples
468 libraries were balanced for the number of estimated reads per cell and run on an Illumina NovaSeq
469 system. Cell Ranger software version 3.1.0 was then used to perform demultiplexing, alignment, filtering,
470 barcode counting, UMI counting, and gene expression estimation for each sample according to the 10x
471 Genomics documentation ([https://support.10xgenomics.com/single-cell-gene-](https://support.10xgenomics.com/single-cell-gene-expression/software/pipelines/latest/what-is-cell-ranger)
472 [expression/software/pipelines/latest/ what-is-cell-ranger](https://support.10xgenomics.com/single-cell-gene-expression/software/pipelines/latest/what-is-cell-ranger)). The reference for alignment was the curated 10x
473 genomics reference for mouse (mm10-3.0.0). The gene expression estimates from each sample were then
474 aggregated using Cellranger (cellranger aggr) to compare experimental groups with normalized
475 sequencing-depth and expression data.

476
477 Single-cell expression data was then analyzed using Seurat 4.0 (Hao et al., 2021). Genes detected in
478 fewer than 5 cells were filtered out of analysis. Doublets were removed from analysis, and cells with
479 <2000 or >20,000 unique molecular identifiers (UMI) or <1000 or >3000 genes were excluded from
480 analysis. Cells with elevated percentage of mitochondrial reads (>5%) were also excluded as a means to

481 **filter out dying cells.** Ultimately 70.0% of cells IN and 80.1% of cells SC passed quality control filters.
482 Data were normalized using the NormalizeData function, and IN and SC samples were integrated for
483 downstream analysis using FindIntegrationAnchors and IntegrateData functions with methods described
484 previously (Stuart et al., 2019). Clustering and visualization for the integrated dataset proceeded with a
485 standard scRNAseq workflow including ScaleData, RunPCA, RunUMAP, FindNeighbors and
486 FindClusters functions. FindClusters was run with resolution parameter 0.83 to achieve clusters that
487 separated cell populations with previously established markers. Cluster markers were obtained with
488 FindMarkers function (min.pct = 0.25). Dimension-reduced plots were generated with FeaturePlot
489 function, splitting by original sample identity as needed for specific analyses. Heatmaps were produced
490 with DoHeatmap function using cluster averages across both experiments calculated with
491 AverageExpression function. Bar plots and scatterplots were generated using R package ggplot2. **Gene set**
492 **enrichment analysis was performed using the clusterProfiler R package using the CellMarker set of mouse**
493 **cell type markers (Wu et al., 2021; Zhang et al., 2019). Specifically, the clusterProfiler function “GSEA”**
494 **was run using a list of genes sorted by descending log2 fold change from the comparison of cells in one**
495 **cluster vs. all others, as calculated by the Seurat FindMarkers function (logfc.threshold = 0). Scoring and**
496 **prediction of cell cycle stage was performed using the Seurat CellCycleScoring function, with the lists of**
497 **S and G2M genes provided by Seurat.**
498
499 **TCR usage analysis.** TCR sequence data was analyzed using TRUST4 v1.0.4.(Song *et al.*, 2021)
500 TRUST4 was run on the position sorted BAM file for each sample generated by CellRanger, along with
501 the V/D/J/C gene reference files provided by TRUST4 (“GRCm38_bcrtr.fa” and “mouse_IMGTC+C.fa”),
502 and the “--barcode CB” option to make clonotype calls for individual cells. The resulting
503 “barcode_report.tsv” output files, which report the most abundant pair of alpha and beta chains for each
504 cell, were summarized within R. The TRUST4 output was filtered for those cells that were retained in the
505 Seurat analysis and for which the predicted cell type was “abT”. For both the alpha and beta chains, the
506 clonotype was defined as the concatenation of the V and J segments, due to limited calls for the D

507 segment of beta chains. Relative frequencies of clonotypes were computed at both the sample and
508 individual cluster level.

509
510 **RNA velocity analysis.** Unspliced and splice read counts were computed using velocity v0.17.17 (La
511 Manno *et al.*, 2018). As input for each sample, velocity (with the “run10x” command) was given the
512 output directory of CellRanger, the CellRanger mouse reference gene annotation (mm10, v3.0.0), and an
513 annotation of repetitive elements for the mouse genome (mm10 RepeatMasker track downloaded from the
514 UCSC Genome Browser in GTF format) (Navarro Gonzalez *et al.*, 2021). The resulting read counts were
515 analyzed with the scVelo v0.2.4 Python package (Bergen *et al.*, 2020). Cells were filtered to those that
516 were analyzed with Seurat and annotated with the Seurat-computed clusters. After standard
517 preprocessing documented by scVelo, velocities were computed using its “stochastic” model. Genes with
518 velocities that were significantly higher in one cluster compared to cells from all other clusters were
519 identified using the “rank_velocity_genes” method (with min_corr =0.3).

520
521 **RT-qPCR experiments.** CD4⁺Tetramer⁺ cells were harvested from lung and spleen following
522 vaccination and pathogen challenge described above. The lungs were processed, stained, and sorted in the
523 same manner as explained before for scRNAseq. Spleens were mashed through 40 µm filters, and then
524 subjected to red blood cell lysis (ACK buffer, Gibco™, Cat#A1049201) for 3 minutes at room
525 temperature. Samples were washed with 15 mL of wash buffer (RPMI with 1% FBS) and the CD4⁺ T
526 cells were enriched using MojoSort™ Mouse CD4 cell isolation (Biolegend, Cat#480006). The cells were
527 stained and sorted as explained before in scRNAseq section as well. Both lungs and spleen were sorted in
528 1.5 ml microtubes with 0.5% BSA in PBS 30 minutes after surface staining and kept at 4°C. Lung and
529 spleen cells were not fixed after surface staining and sorted in sterile condition in order to perform *in vitro*
530 stimulation experiments. The samples were pooled after surface staining step (3-4 mice/sample, total of 3
531 samples).

532

533 For stimulation studies, cells from lung or spleen (50,000-200,000 cells/well) were left unstimulated
534 (RPMI with 0.5% BSA) or stimulated with IFN α (10,000 units/mL) or IFN γ (10 ng/ml) and analyzed by
535 RT-qPCR at 12 hours. To measure mRNA expression levels of genes, cDNA was generated directly from
536 cell lysate using the Invitrogen SuperScript IV CellsDirect cDNA Synthesis Kit (ThermoFisher Scientific,
537 11750150). qPCR was performed on a Rotor-Gene Q system (Qiagen) using TaqMan Gene Expression
538 Assays (ThermoFisher Scientific, Ifi204 Mm00492602_m1; Mx1 Mm00487796_m1; Pml
539 Mm00476969_m1; Slfn5 Mm00806095_m1; Ifit1 Mm00515153_m1; Ifitm3 Mm00847057_s1; Il17a
540 Mm00439618_m1; 18S 4319413E) and TaqMan Fast Advanced Master Mix (ThermoFisher Scientific,
541 4444556). Relative quantification was performed by the $\Delta\Delta$ CT method with 18S as a reference gene.
542 Relative expression levels were compared using data from one experiment representative of three
543 independent experiments using two-tailed Student's t-test.

544
545 **Data Availability.** Raw and integrated scRNAseq data is deposited in Gene Expression Omnibus (GEO)
546 database, [with accession number GSE198466](#).

547

548 **ACKNOWLEDGMENTS**

549 The authors thank Dr. Jenny Gumperz for her insight and expertise regarding natural killer T
550 cells and the University of Wisconsin-Madison Clinical Cancer Center, Flow Cytometry Core
551 Facility (UWCCC) and Biotechnology Center for help with cell sorting and sequencing. Robert
552 Gordon (Department of Pediatrics) assisted with graphic illustration. The UWCCC is supported
553 by NIH Shared Instrumentation Grant 1S100OD018202–01 and University of Wisconsin
554 Carbone Cancer Center Support grant P30 CA014520. We also acknowledge support from NIH
555 grants R01 AI130411, U01AI124299, R01 AI035681 (to B.K.); R01AI168370 (to B.K. and
556 M.W.); R01 AI093553 (to M.W.); the University of Wisconsin-Madison Institutional Clinical and
557 Translational Science Award UL1 TR002373 (to C.D.); and from the University of Wisconsin School
558 of Medicine and Public Health Pediatrics Fellow/Resident research grant (to T.W.). Xin He is a
559 Cancer Research Institute Irvington Fellow supported by the Cancer Research Institute
560 (CRI4476). Bruce Klein is a CIFAR Fellow and receives support from this agency.

561 **REFERENCES**

- 562 Andreatta, M., Corria-Osorio, J., Müller, S., Cubas, R., Coukos, G., and Carmona, S.J. (2021).
563 Interpretation of T cell states from single-cell transcriptomics data using reference atlases. *Nat*
564 *Commun* *12*, 2965. 10.1038/s41467-021-23324-4.
- 565 Arazi, A., Rao, D.A., Berthier, C.C., Davidson, A., Liu, Y., Hoover, P.J., Chicoine, A., Eisenhaure, T.M.,
566 Jonsson, A.H., Li, S., et al. (2019). The immune cell landscape in kidneys of patients with lupus
567 nephritis. *Nat Immunol* *20*, 902-914. 10.1038/s41590-019-0398-x.
- 568 Bach, E.A., Aguet, M., and Schreiber, R.D. (1997). The IFN gamma receptor: a paradigm for cytokine
569 receptor signaling. *Annu Rev Immunol* *15*, 563-591. 10.1146/annurev.immunol.15.1.563.
- 570 Bach, E.A., Szabo, S.J., Dighe, A.S., Ashkenazi, A., Aguet, M., Murphy, K.M., and Schreiber, R.D.
571 (1995). Ligand-induced autoregulation of IFN-gamma receptor beta chain expression in T helper cell
572 subsets. *Science* *270*, 1215-1218. 10.1126/science.270.5239.1215.
- 573 Bergen, V., Lange, M., Peidli, S., Wolf, F.A., and Theis, F.J. (2020). Generalizing RNA velocity to
574 transient cell states through dynamical modeling. *Nat Biotechnol* *38*, 1408-1414. 10.1038/s41587-020-
575 0591-3.
- 576 Cheng, N., Janumyan, Y.M., Didion, L., Van Hofwegen, C., Yang, E., and Knudson, C.M. (2004). Bcl-2
577 inhibition of T-cell proliferation is related to prolonged T-cell survival. *Oncogene* *23*, 3770-3780.
578 10.1038/sj.onc.1207478.
- 579 Debes, G.F., Arnold, C.N., Young, A.J., Krautwald, S., Lipp, M., Hay, J.B., and Butcher, E.C. (2005).
580 Chemokine receptor CCR7 required for T lymphocyte exit from peripheral tissues. *Nat Immunol* *6*,
581 889-894. 10.1038/ni1238.
- 582 Dobson, H.E., Dias, L.D.S., Kohn, E.M., Fites, S., Wiesner, D.L., Dileepan, T., Kujoth, G.C., Abraham,
583 A., Ostroff, G.R., Klein, B.S., and Wüthrich, M. (2020). Antigen discovery unveils resident memory
584 and migratory cell roles in antifungal resistance. *Mucosal Immunol* *13*, 518-529. 10.1038/s41385-019-
585 0244-3.
- 586 Duclos, P., Okwo-Bele, J.M., Gacic-Dobo, M., and Cherian, T. (2009). Global immunization: status,
587 progress, challenges and future. *BMC Int Health Hum Rights* *9 Suppl 1*, S2. 10.1186/1472-698X-9-S1-
588 S2.
- 589 Eberl, G., Lees, R., Smiley, S.T., Taniguchi, M., Grusby, M.J., and MacDonald, H.R. (1999). Tissue-
590 specific segregation of CD1d-dependent and CD1d-independent NK T cells. *J Immunol* *162*, 6410-
591 6419.
- 592 Emming, S., Bianchi, N., Polletti, S., Balestrieri, C., Leoni, C., Montagner, S., Chirichella, M., Delaleu,
593 N., Natoli, G., and Monticelli, S. (2020). A molecular network regulating the proinflammatory
594 phenotype of human memory T lymphocytes. *Nat Immunol* *21*, 388-399. 10.1038/s41590-020-0622-8.
- 595 Engel, I., Seumois, G., Chavez, L., Samaniego-Castruita, D., White, B., Chawla, A., Mock, D.,
596 Vijayanand, P., and Kronenberg, M. (2016). Innate-like functions of natural killer T cell subsets result
597 from highly divergent gene programs. *Nat Immunol* *17*, 728-739. 10.1038/ni.3437.
- 598 Everitt, A.R., Clare, S., Pertel, T., John, S.P., Wash, R.S., Smith, S.E., Chin, C.R., Feeley, E.M., Sims,
599 J.S., Adams, D.J., et al. (2012). IFITM3 restricts the morbidity and mortality associated with influenza.
600 *Nature* *484*, 519-523. 10.1038/nature10921.
- 601 Farr, A.R., Wu, W., Choi, B., Cavalcoli, J.D., and Laouar, Y. (2014). CD1d-unrestricted NKT cells are
602 endowed with a hybrid function far superior than that of iNKT cells. *Proc Natl Acad Sci U S A* *111*,
603 12841-12846. 10.1073/pnas.1323405111.
- 604 Galvani, A., Modhadas, S., and Schneider, E. (2021). Deaths and Hospitalizations Averted by Rapid US
605 Vaccine Rollout. [https://www.commonwealthfund.org/publications/issue-briefs/2021/jul/deaths-and-](https://www.commonwealthfund.org/publications/issue-briefs/2021/jul/deaths-and-hospitalizations-averted-rapid-us-vaccination-rollout)
606 [hospitalizations-averted-rapid-us-vaccination-rollout](https://www.commonwealthfund.org/publications/issue-briefs/2021/jul/deaths-and-hospitalizations-averted-rapid-us-vaccination-rollout).
- 607 Garg, A.V., Amatya, N., Chen, K., Cruz, J.A., Grover, P., Whibley, N., Conti, H.R., Hernandez Mir, G.,
608 Sirakova, T., Childs, E.C., et al. (2015). MCPIP1 Endoribonuclease Activity Negatively Regulates
609 Interleukin-17-Mediated Signaling and Inflammation. *Immunity* *43*, 475-487.
610 10.1016/j.immuni.2015.07.021.

- 611 Giroux, M., and Denis, F. (2005). CD1d-unrestricted human NKT cells release chemokines upon Fas
612 engagement. *Blood* *105*, 703-710. 10.1182/blood-2004-04-1537.
- 613 Godfrey, D.I., MacDonald, H.R., Kronenberg, M., Smyth, M.J., and Van Kaer, L. (2004). NKT cells:
614 what's in a name? *Nat Rev Immunol* *4*, 231-237. 10.1038/nri1309.
- 615 Gowthaman, U., Chen, J.S., Zhang, B., Flynn, W.F., Lu, Y., Song, W., Joseph, J., Gertie, J.A., Xu, L.,
616 Collet, M.A., et al. (2019). Identification of a T follicular helper cell subset that drives anaphylactic
617 IgE. *Science* *365*. 10.1126/science.aaw6433.
- 618 Hao, Y., Hao, S., Andersen-Nissen, E., Mauck, W.M., Zheng, S., Butler, A., Lee, M.J., Wilk, A.J., Darby,
619 C., Zager, M., et al. (2021). Integrated analysis of multimodal single-cell data. *Cell* *184*, 3573-
620 3587.e3529. 10.1016/j.cell.2021.04.048.
- 621 Harsha Krovi, S., Zhang, J., Michaels-Foster, M.J., Brunetti, T., Loh, L., Scott-Browne, J., and Gapin, L.
622 (2020). Thymic iNKT single cell analyses unmask the common developmental program of mouse
623 innate T cells. *Nat Commun* *11*, 6238. 10.1038/s41467-020-20073-8.
- 624 Heaton, P.M. (2020). Challenges of Developing Novel Vaccines With Particular Global Health
625 Importance. *Front Immunol* *11*, 517290. 10.3389/fimmu.2020.517290.
- 626 Huppler, A.R., Bishu, S., and Gaffen, S.L. (2012). Mucocutaneous candidiasis: the IL-17 pathway and
627 implications for targeted immunotherapy. *Arthritis Res Ther* *14*, 217. 10.1186/ar3893.
- 628 Kiner, E. (2019). Heterogeneity of CD4⁺ T cells. <http://nrs.harvard.edu/urn-3:HUL.InstRepos:42029758>.
- 629 Kiner, E., Willie, E., Vijaykumar, B., Chowdhary, K., Schmutz, H., Chandler, J., Schnell, A., Thakore,
630 P.I., LeGros, G., Mostafavi, S., et al. (2021). Gut CD4⁺ T cell phenotypes are a continuum molded by
631 microbes, not by T_H archetypes. *Nat Immunol* *22*, 216-228. 10.1038/s41590-020-00836-7.
- 632 La Manno, G., Soldatov, R., Zeisel, A., Braun, E., Hochgerner, H., Petukhov, V., Lidschreiber, K.,
633 Kastrioti, M.E., Lönnerberg, P., Furlan, A., et al. (2018). RNA velocity of single cells. *Nature* *560*, 494-
634 498. 10.1038/s41586-018-0414-6.
- 635 Mao, A.P., Ishizuka, I.E., Kasal, D.N., Mandal, M., and Bendelac, A. (2017). A shared Runx1-bound
636 Zbtb16 enhancer directs innate and innate-like lymphoid lineage development. *Nat Commun* *8*, 863.
637 10.1038/s41467-017-00882-0.
- 638 Matsushita, K., Takeuchi, O., Standley, D.M., Kumagai, Y., Kawagoe, T., Miyake, T., Satoh, T., Kato,
639 H., Tsujimura, T., Nakamura, H., and Akira, S. (2009). Zc3h12a is an RNase essential for controlling
640 immune responses by regulating mRNA decay. *Nature* *458*, 1185-1190. 10.1038/nature07924.
- 641 Merkhofer, R.M., O'Neill, M.B., Xiong, D., Hernandez-Santos, N., Dobson, H., Fites, J.S., Shockey,
642 A.C., Wuethrich, M., Pepperell, C.S., and Klein, B.S. (2019). Investigation of Genetic Susceptibility to
643 Blastomycosis Reveals Interleukin-6 as a Potential Susceptibility Locus. *mBio* *10*.
644 10.1128/mBio.01224-19.
- 645 Miragaia, R.J., Gomes, T., Chomka, A., Jardine, L., Riedel, A., Hegazy, A.N., Whibley, N., Tucci, A.,
646 Chen, X., Lindeman, I., et al. (2019). Single-Cell Transcriptomics of Regulatory T Cells Reveals
647 Trajectories of Tissue Adaptation. *Immunity* *50*, 493-504.e497. 10.1016/j.immuni.2019.01.001.
- 648 Monaco, G., Lee, B., Xu, W., Mustafah, S., Hwang, Y.Y., Carre, C., Burdin, N., Visan, L., Ceccarelli, M.,
649 Poidinger, M., et al. (2019). RNA-Seq Signatures Normalized by mRNA Abundance Allow Absolute
650 Deconvolution of Human Immune Cell Types. *Cell Rep* *26*, 1627-1640 e1627.
651 10.1016/j.celrep.2019.01.041.
- 652 Morris, R., Kershaw, N.J., and Babon, J.J. (2018). The molecular details of cytokine signaling via the
653 JAK/STAT pathway. *Protein Sci* *27*, 1984-2009. 10.1002/pro.3519.
- 654 Navarro Gonzalez, J., Zweig, A.S., Speir, M.L., Schmelter, D., Rosenbloom, K.R., Raney, B.J., Powell,
655 C.C., Nassar, L.R., Maulding, N.D., Lee, C.M., et al. (2021). The UCSC Genome Browser database:
656 2021 update. *Nucleic Acids Res* *49*, D1046-D1057. 10.1093/nar/gkaa1070.
- 657 Ng, S.S., De Labastida Rivera, F., Yan, J., Corvino, D., Das, I., Zhang, P., Kuns, R., Chauhan, S.B., Hou,
658 J., Li, X.Y., et al. (2020). The NK cell granule protein NKG7 regulates cytotoxic granule exocytosis
659 and inflammation. *Nat Immunol* *21*, 1205-1218. 10.1038/s41590-020-0758-6.

- 660 Ortiz, B.D., Krensky, A.M., and Nelson, P.J. (1996). Kinetics of transcription factors regulating the
661 RANTES chemokine gene reveal a developmental switch in nuclear events during T-lymphocyte
662 maturation. *Mol Cell Biol* *16*, 202-210. 10.1128/MCB.16.1.202.
- 663 Panagioti, E., Klenerman, P., Lee, L.N., van der Burg, S.H., and Arens, R. (2018). Features of Effective T
664 Cell-Inducing Vaccines against Chronic Viral Infections. *Front Immunol* *9*, 276.
665 10.3389/fimmu.2018.00276.
- 666 Pollard, A.J., and Bijker, E.M. (2021). A guide to vaccinology: from basic principles to new
667 developments. *Nat Rev Immunol* *21*, 83-100. 10.1038/s41577-020-00479-7.
- 668 Prelli Bozzo, C., Nchioua, R., Volcic, M., Koepke, L., Krüger, J., Schütz, D., Heller, S., Stürzel, C.M.,
669 Kmiec, D., Conzelmann, C., et al. (2021). IFITM proteins promote SARS-CoV-2 infection and are
670 targets for virus inhibition in vitro. *Nat Commun* *12*, 4584. 10.1038/s41467-021-24817-y.
- 671 Rezende, R.M., and Weiner, H.L. (2017). History and mechanisms of oral tolerance. *Semin Immunol* *30*,
672 3-11. 10.1016/j.smim.2017.07.004.
- 673 Schenkel, J.M., and Masopust, D. (2014). Tissue-resident memory T cells. *Immunity* *41*, 886-897.
674 10.1016/j.immuni.2014.12.007.
- 675 Seo, W., Shimizu, K., Kojo, S., Okeke, A., Kohwi-Shigematsu, T., Fujii, S.I., and Taniuchi, I. (2020).
676 Runx-mediated regulation of CCL5 via antagonizing two enhancers influences immune cell function
677 and anti-tumor immunity. *Nat Commun* *11*, 1562. 10.1038/s41467-020-15375-w.
- 678 Seumois, G., Ramírez-Suástegui, C., Schmiedel, B.J., Liang, S., Peters, B., Sette, A., and Vijayanand, P.
679 (2020). Single-cell transcriptomic analysis of allergen-specific T cells in allergy and asthma. *Sci*
680 *Immunol* *5*. 10.1126/sciimmunol.aba6087.
- 681 Singhania, A., Graham, C.M., Gabryšová, L., Moreira-Teixeira, L., Stavropoulos, E., Pitt, J.M.,
682 Chakravarty, P., Warnatsch, A., Branchett, W.J., Conejero, L., et al. (2019). Transcriptional profiling
683 unveils type I and II interferon networks in blood and tissues across diseases. *Nat Commun* *10*, 2887.
684 10.1038/s41467-019-10601-6.
- 685 Smith, T., Heger, A., and Sudbery, I. (2017). UMI-tools: modeling sequencing errors in Unique
686 Molecular Identifiers to improve quantification accuracy. *Genome Res* *27*, 491-499.
687 10.1101/gr.209601.116.
- 688 Song, L., Cohen, D., Ouyang, Z., Cao, Y., Hu, X., and Liu, X.S. (2021). TRUST4: immune repertoire
689 reconstruction from bulk and single-cell RNA-seq data. *Nat Methods* *18*, 627-630. 10.1038/s41592-
690 021-01142-2.
- 691 Speakman, E.A., Dambuza, I.M., Salazar, F., and Brown, G.D. (2020). T Cell Antifungal Immunity and
692 the Role of C-Type Lectin Receptors. *Trends Immunol* *41*, 61-76. 10.1016/j.it.2019.11.007.
- 693 Stuart, T., Butler, A., Hoffman, P., Hafemeister, C., Papalexi, E., Mauck, W.M., Hao, Y., Stoeckius, M.,
694 Smibert, P., and Satija, R. (2019). Comprehensive Integration of Single-Cell Data. *Cell* *177*, 1888-
695 1902.e1821. 10.1016/j.cell.2019.05.031.
- 696 Stubbington, M.J.T., Rozenblatt-Rosen, O., Regev, A., and Teichmann, S.A. (2017). Single-cell
697 transcriptomics to explore the immune system in health and disease. *Science* *358*, 58-63.
698 10.1126/science.aan6828.
- 699 Szabo, P.A., Levitin, H.M., Miron, M., Snyder, M.E., Senda, T., Yuan, J., Cheng, Y.L., Bush, E.C.,
700 Dogra, P., Thapa, P., et al. (2019). Single-cell transcriptomics of human T cells reveals tissue and
701 activation signatures in health and disease. *Nat Commun* *10*, 4706. 10.1038/s41467-019-12464-3.
- 702 Takeuchi, A., and Saito, T. (2017). CD4 CTL, a Cytotoxic Subset of CD4(+) T Cells, Their
703 Differentiation and Function. *Front Immunol* *8*, 194. 10.3389/fimmu.2017.00194.
- 704 The Human Protein Atlas (2019). RGS16 Immune Cell Type Expression, Monaco dataset.
705 <https://www.proteinatlas.org/ENSG00000143333-RGS16/immune+cell>.
- 706 Tibbitt, C.A., Stark, J.M., Martens, L., Ma, J., Mold, J.E., Deswarte, K., Oliynyk, G., Feng, X.,
707 Lambrecht, B.N., De Bleser, P., et al. (2019). Single-Cell RNA Sequencing of the T Helper Cell
708 Response to House Dust Mites Defines a Distinct Gene Expression Signature in Airway Th2 Cells.
709 *Immunity* *51*, 169-184.e165. 10.1016/j.immuni.2019.05.014.

710 Wu, T., Hu, E., Xu, S., Chen, M., Guo, P., Dai, Z., Feng, T., Zhou, L., Tang, W., Zhan, L., et al. (2021).
711 clusterProfiler 4.0: A universal enrichment tool for interpreting omics data. *Innovation (Camb)* 2,
712 100141. 10.1016/j.xinn.2021.100141.
713 Zemmour, D., Kiner, E., and Benoist, C. (2020). CD4⁺ T_{eff} heterogeneity: the perspective from single-cell
714 transcriptomics. *Curr Opin Immunol* 63, 61-67. 10.1016/j.coi.2020.02.004.
715 Zemmour, D., Zilionis, R., Kiner, E., Klein, A.M., Mathis, D., and Benoist, C. (2018). Single-cell gene
716 expression reveals a landscape of regulatory T cell phenotypes shaped by the TCR. *Nat Immunol* 19,
717 291-301. 10.1038/s41590-018-0051-0.
718 Zhang, M.J., Ntranos, V., and Tse, D. (2020). Determining sequencing depth in a single-cell RNA-seq
719 experiment. *Nat Commun* 11, 774. 10.1038/s41467-020-14482-y.
720 Zhang, X., Lan, Y., Xu, J., Quan, F., Zhao, E., Deng, C., Luo, T., Xu, L., Liao, G., Yan, M., et al. (2019).
721 CellMarker: a manually curated resource of cell markers in human and mouse. *Nucleic Acids Res* 47,
722 D721-D728. 10.1093/nar/gky900.
723 Zhu, J., and Paul, W.E. (2010). Heterogeneity and plasticity of T helper cells. *Cell Res* 20, 4-12.
724 10.1038/cr.2009.138.
725

726 **FIGURE LEGENDS**

727 **Figure 1. Single-cell RNAseq analysis of tetramer-positive T cells in *Blastomyces*-challenged mice**
728 **following subcutaneous (SC) or intranasal (IN) vaccination. (a)** Experimental schema for IN and SC
729 vaccination with *Blastomyces* endoglucanase-2 (BI-Eng2), lethal experimental challenge with
730 *Blastomyces*, sorting of BI-Eng2-specific CD4⁺ T cells with tetramer, and single-cell RNAseq. **(b)** Gating
731 strategy for selection of tetramer⁺ CD4⁺ T cells. Representative flow cytometry plots shown for the SC
732 group cells; see Supplemental Figure 1 for IN group flow cytometry plots. **(c)** Uniform manifold
733 approximation and projection (UMAP) for integrated analysis of SC and IN group cells yields 16 distinct
734 cell clusters. Cluster numbers are assigned based on largest population (cluster 1) to smallest (cluster 16).

735
736 **Figure 2. Identities of scRNAseq clusters. (a)** Expression of CD4⁺ T cell genes (*Trac*, *Cd3d*) is
737 consistent with gating strategy at the protein level across all 16 clusters. **(b)** UMAPs for T_{RM} markers
738 *Cd69*, *Lgas11*, *Lgals2*, and *Vim* show nonspecific expression patterns across most clusters. **(c)** UMAPs for
739 resting (naïve/T_{CM}) markers *Ccr7* and *Sell* show expression localizing to clusters 9 and 16. **(d)** Heatmap
740 showing average expression and percent of cells expressing key genes to assign cluster identities. Marker
741 genes include known lymphocyte marker genes and top differentially expressed genes identified as cluster
742 markers by the scRNAseq package Seurat. Abbreviations: Tis T = Type I interferon signature T cells;
743 NK-Th1 = NK-like Th1 cells; MyT = myeloid-like T cells.

744
745 **Figure 3. Differences in relative cluster abundance and gene expression between IN and SC**
746 **vaccinated mice. (a)** UMAP of 16 cell clusters separated by IN and SC sample origin, showing shifts in
747 relative cluster abundance between these two groups. **(b)** Scatterplot of relative proportions of each
748 cluster within all IN group cells (x-axis) and SC group cells (y-axis). Clusters falling above dotted line
749 have higher relative abundance for SC group; clusters below dotted line have higher relative abundance
750 for IN group. Those with >2x increased relative abundance in IN or SC samples are green and purple,
751 respectively; cluster 16 made up <1% of all cells and was not color coded. **(c)** Dot plot of key genes with
752 differential expression between IN and SC samples, grouped by functional similarity (colored annotation

753 to the right of panel); all with exception of *Lag3* and *Pdcd1* are significantly different ($p < 0.05$). High
754 and low activation gene lists are adapted from scRNAseq profiling of CD4⁺ T cells elsewhere (see Kiner
755 et al., e.g. Fig 1d.). **(d)** UMAP for activation-induced immune checkpoint gene *Ctla4*. Circled clusters 4, 5
756 and 13 are shown in detail with the violin plot for *Ctla4* expression in **(e)**, where these clusters show
757 decreased expression SC compared to IN. This difference contrasts with stable *Ctla4* expression in Tregs
758 in both IN and SC groups. **(f)** UMAP for *Il17a* and *Ifng*, separated by IN and SC groups. **(g)** Number of
759 cells within each cluster expressing *Il17a* only, *Ifng* only, both *Il17a* and *Ifng*, or neither cytokine. Note
760 the switch in dominant cytokine from *Il17a* to *Ifng* within certain clusters (e.g. cluster 3) depending on
761 vaccine exposure route.

762
763 **Figure 4. TCR clonotype diversity in IN and SC vaccinated mice.** **(a)** Relative abundance of TCR α , β ,
764 and $\alpha\beta$ chain clonotypes identified by TRUST4 in IN and SC samples. **(b)** TCR α -chain clonotypes vary
765 in relative abundance between IN and SC samples. Only clonotypes with >2% abundance in either sample
766 are shown. **(c)** Distribution of the top 5 TCR α -chain clonotypes across each cluster. The size of each
767 circle depicts the number of cells expressing each clonotype per cluster. The color represents how
768 relatively enriched (red) or depleted (blue) that cluster is for a given clonotype. White color indicates that
769 the frequency of the clonotype is the same as the frequency across the entire sample.

770
771 **Figure 5. Tregs and NK-like Th1 cells in IN and SC vaccinated mice.** **(a)** Relative abundance of Tregs
772 in IN and SC samples, expressed as percent of total cells in each sample. **(b)** Violin plot showing average
773 expression of tolerogenic Treg cytokines *Tgfb1* (TGF β), *Il10* (IL-10), and *Il4* (IL-4), IN compared to SC.
774 **(c)** Relative abundance of cluster 12 cells (NK-like Th1) in IN and SC samples, expressed as percent of
775 total cells in each sample. **(d)** UMAP for *Nkg7*, an NK marker highly expressed in multiple SC-enriched
776 populations including cluster 12. **(e)** UMAP for chemokine *Ccl5*, showing focal expression by cluster 12
777 cells. **(f)** Heatmap of average cluster expression of NKT1 marker genes identified in thymic Cd1d
778 tetramer-positive cells (see: Engel et al., Figure 5). (Engel *et al.*, 2016) Markers are primarily upregulated
779 in NKT1 cells but include a subset of 4 genes downregulated in NKT1 (*Atp1f1*, *Ckb*, *Rexo2*, *Emb*).

780
781 **Figure 6. Tis T cell phenotypes in IN and SC vaccinated mice.** (a) Relative abundance of Tis T cells in
782 IN and SC samples, expressed as percent of total cells in each sample. (b) UMAP for expression of type I
783 interferon response genes, localizing Tis T cells to clusters 8 and 13. (c) Heatmap showing average
784 expression and percent of cells expressing Tis T cell markers noted in the literature (e.g. *Isg15*, *Isg20*,
785 *Mx1*, *Rsad2*, *Oas3*, *Ifit1*, *Ifit3*) and identified as markers for both clusters by scRNAseq differential
786 expression analysis. (d) Heatmap for genes differing between the two clusters of Tis T cells. Red and blue
787 side bars represent those genes that are upregulated or downregulated in the first principal component
788 (PC1) of CD4⁺ T cells harvested after infection with enteric pathogens (*Salmonella typhimurium*,
789 *Citrobacter rodentium*, *Heligmosomoides polygyrus* and *Nippostrongylus brasiliensis*; see Kiner,
790 Supplemental figure 2) (Kiner, 2019). (e) UMAP showing similar patterns in activation gene expression,
791 represented by *Bhlhe40* and *Nfkbia*, between cluster 13 Tis T cells and nearby clusters 4 and 5, both IN
792 and SC.

793
794 **Figure 7. RT-PCR Tis T cell signature.** (a) Quantitative reverse transcriptase PCR (RT-qPCR) detects
795 increased expression of Tis T cell marker genes (*Ifi204*, *Mx1*, *Pml*, *Slfn5*, *Ifit1*, *Ifitm3*) in tetramer-
796 positive, CD44-positive (black) cells compared to control CD44-negative (white) cells from the lungs of
797 *Blastomyces*-challenged, subcutaneously vaccinated mice. The addition of IFN α increased expression of
798 these genes in both tetramer-positive and control cells. (b) Tis T cell signature (*Ifi204*, *Ifitm3*) was
799 increased in SC vaccinated animals compared to IN vaccinated animals by RT-qPCR. (c) Violin plot
800 depicting expression of interferon receptor genes in Tis T cells (clusters 8, 13). While these clusters
801 expressed the IFN γ R α -chain, the corresponding β -chain was not detected. (d) Tis T cell signature is
802 diminished in lungs of *Blastomyces*-challenged, subcutaneously vaccinated mice lacking IFN γ R (IFN γ R-
803 KO) as compared to wild type mice. *, p<0.05; **p<0.01; ***, p<0.001. Analysis by two-way ANOVA.

804 **SUPPLEMENTAL FIGURES**

805 **Supplemental Figure 1.** (a) Flow cytometry plots for selection of tetramer⁺ CD4⁺ T cells from IN
806 sample. (b) Counts of sorted and sequenced tetramer-positive CD4⁺ cells from SC and IN samples. (c)
807 UMAP for cell cycle phases of IN and SC groups. Cells in all stages are distributed across all clusters. (d)
808 UMAP after regression of cell cycle genes in IN and SC groups shows cohesive clusters with both the
809 original cluster assignments prior to regression (top) and the new cluster assignments after regression
810 (bottom). (e) Stacked bar plot depicting relative abundance of each cluster within the IN and SC groups.

811
812 **Supplemental Figure 2.** (a) Heatmap showing average expression of tissue-associated memory T cell
813 genes involved in cytoskeleton, cell matrix, membrane scaffolding and adhesion. Gene list adapted from
814 Szabo et al. (Szabo *et al.*, 2019) The cluster with conspicuous downregulation of these tissue-associated
815 genes corresponds to the naïve/T_{CM} population (cluster 9). (b) Comparison of the number of detected
816 genes and reads in quiescent cells (cluster 11) compared to other clusters. Both were significantly lower
817 in cluster 11 cells (genes, $P=1.5 \times 10^{-174}$; reads, $P=6.1 \times 10^{-103}$). P-values generated with Mann-Whitney test
818 (***) ($P < 0.001$). (c) Less than 5% of reads mapped to mitochondrial genes across all clusters. Cluster 11
819 cells were comparable to other clusters for percent mitochondrial reads. (d) Comparison of the number of
820 detected genes and reads in myeloid-like T cells (MyT, cluster 16) compared to other clusters. There was
821 no significant increase in gene or read counts to suggest doublets within this population (genes, $P=0.17$;
822 reads, $P=0.39$). P-values generated with Mann-Whitney test. (e) UMAP for Th1 transcription factor
823 *Tbx21* (Tbet) and Th17 transcription factor *Rorc* (ROR γ t).

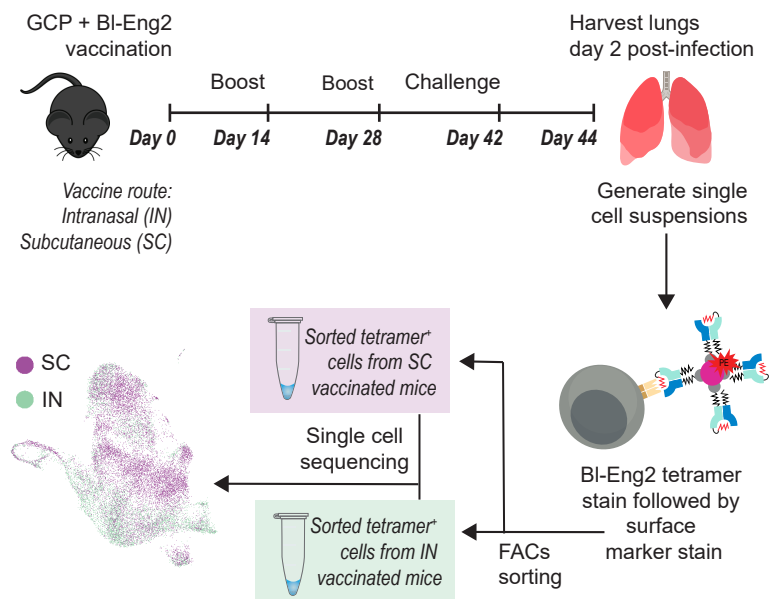
824
825 **Supplemental Figure 3.** (a) Total cells with α , β , or $\alpha\beta$ TCR clonotype calls using TRUST4 in IN and
826 SC samples. (b) Proportion of cells within each cluster with an α , β , or $\alpha\beta$ TCR clonotype call. (c)
827 Frequency of the most abundant α , β , or $\alpha\beta$ TCR clonotype was higher IN than SC groups. (d)
828 Cumulative frequency of the top α , β , or $\alpha\beta$ TCR clonotypes. (e) The proportion of the 5 most abundant
829 TCR α -chain clonotypes within each cluster.

830

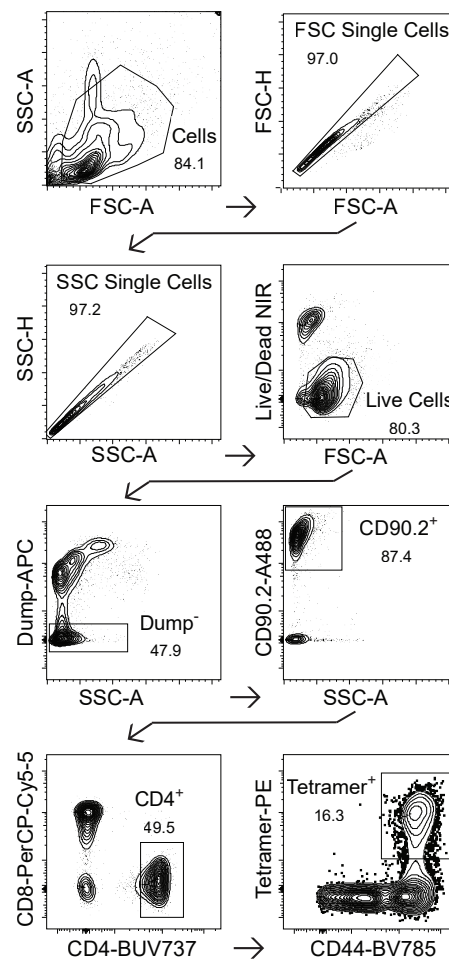
831 **Supplemental Figure 4. (a)** UMAP for expression of T cell anergy gene *Rnf128* (GRAIL), separated by
832 IN and SC samples. **(b)** Violin plot showing lack of expression of innate-like T cell gene *Zbtb16* (PZLF)
833 in NK-like Th1 and all other cells.

834
835 **Supplemental Figure 5. (a)** Quantitative reverse transcriptase PCR (RT-qPCR) detects increased
836 expression of Tis T cell marker genes (*Ifi204*, *Mx1*, *Pml*, *Slfn5*, *Ifit1*) in tetramer-positive, CD44-positive
837 (black) cells compared to control CD44-negative (white) cells from the spleen of *Blastomyces*-challenged,
838 subcutaneously vaccinated mice. The addition of IFN α increased expression of these genes in both
839 tetramer-positive and control cells. **(b)** RT-qPCR for Tis T cell marker genes in tetramer-positive, CD44-
840 positive cells from the spleen of *Blastomyces*-challenged, subcutaneously vaccinated mice do not increase
841 12h after IFN γ stimulation compared to those left unstimulated (Mock). **(c)** RT-qPCR for *Ifit3* in
842 tetramer-positive, CD44-positive cells from the lungs of *Blastomyces*-challenged, subcutaneously
843 vaccinated mice do not increase 12h after IFN γ stimulation compared to those left unstimulated (Mock).
844 **(d)** Percentage of CD4⁺ T cells and tetramer-positive T cells harvested from the lungs of IFN γ R^{-/-} (KO)
845 mice and wild-type mice that were vaccinated SC, experimentally challenged via the pulmonary route,
846 and analyzed three days post-infection.

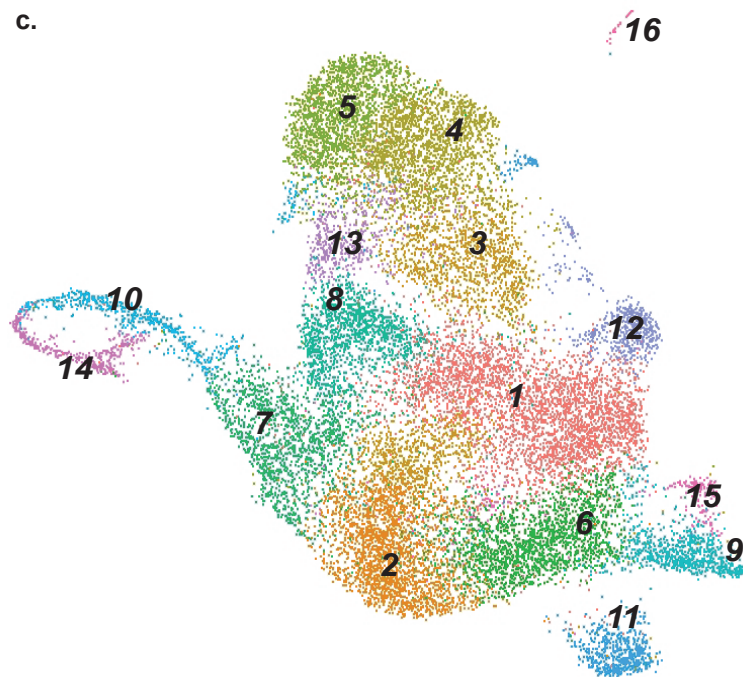
a.

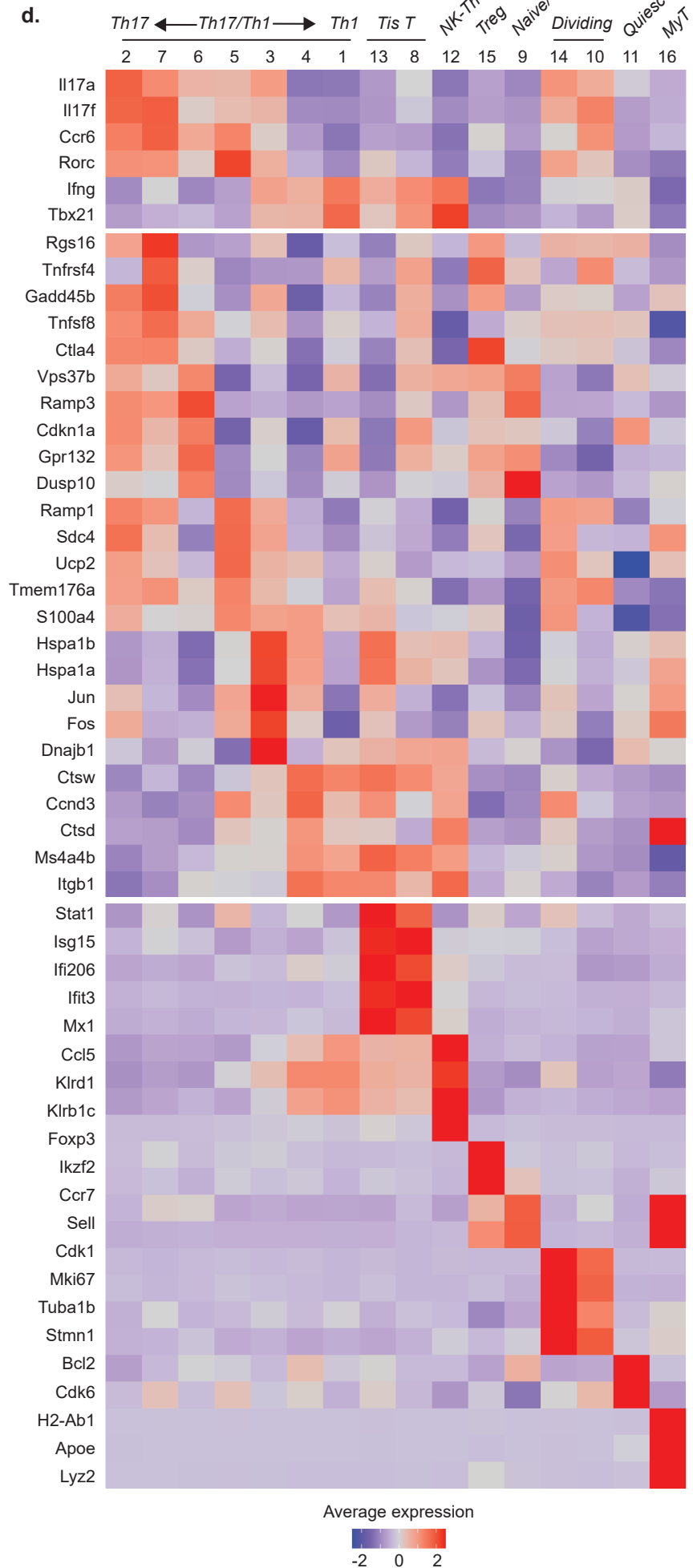
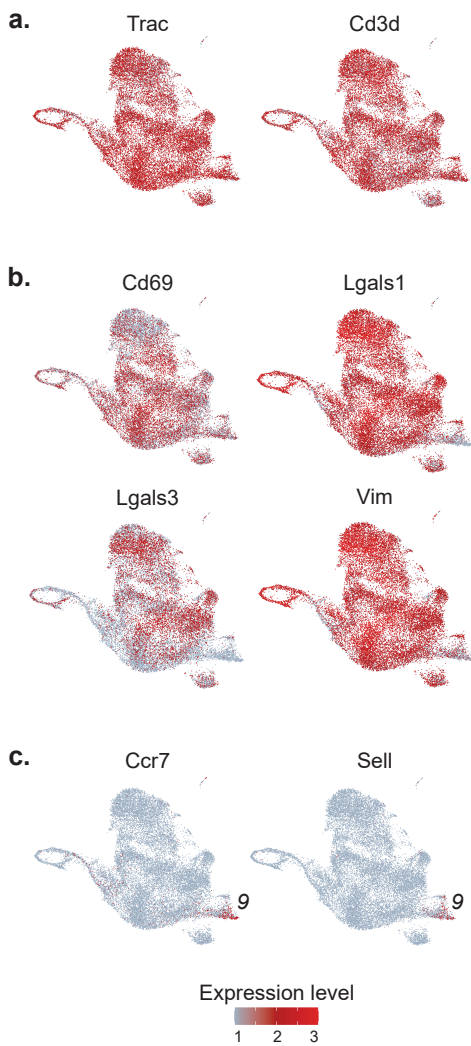


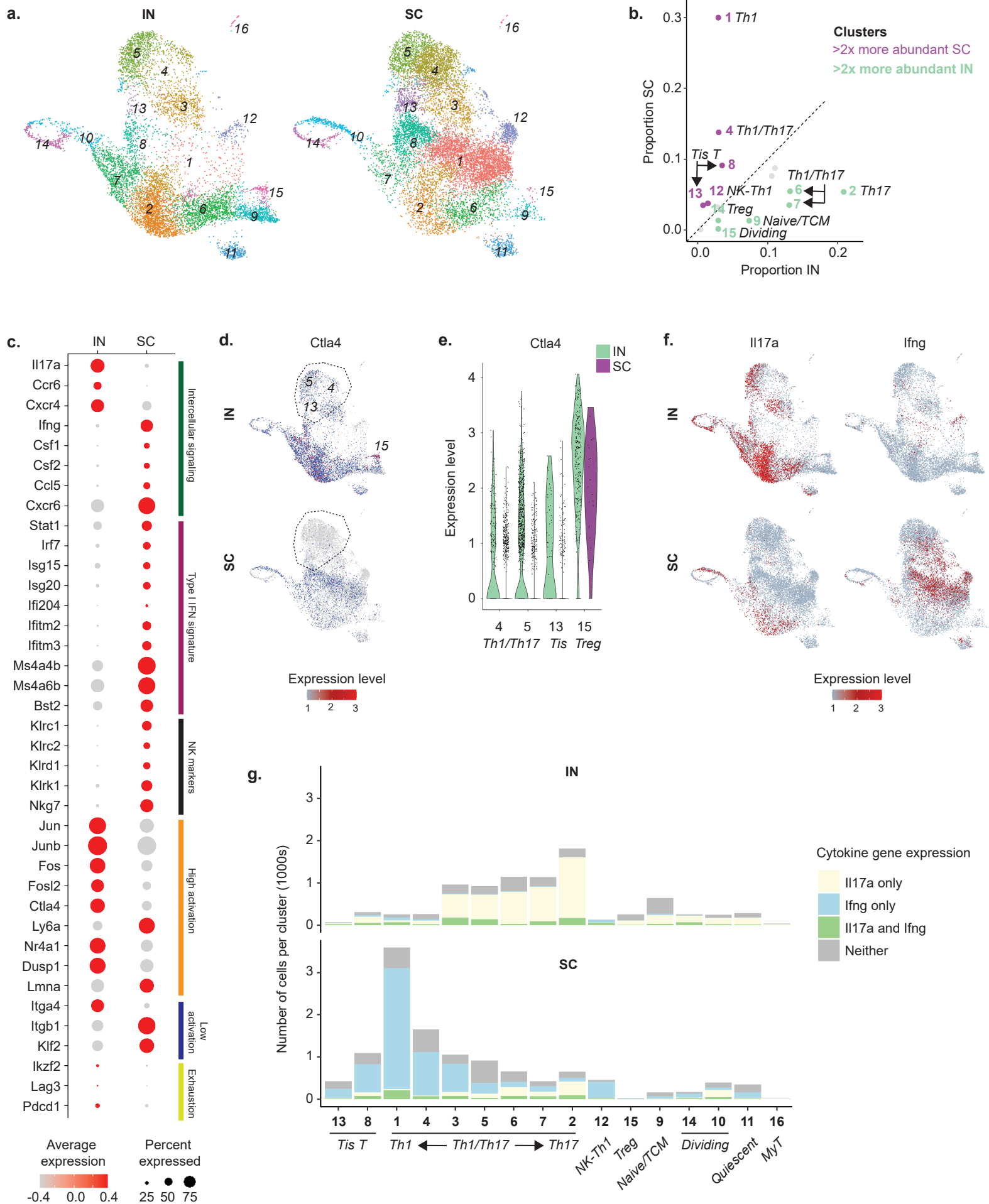
b.

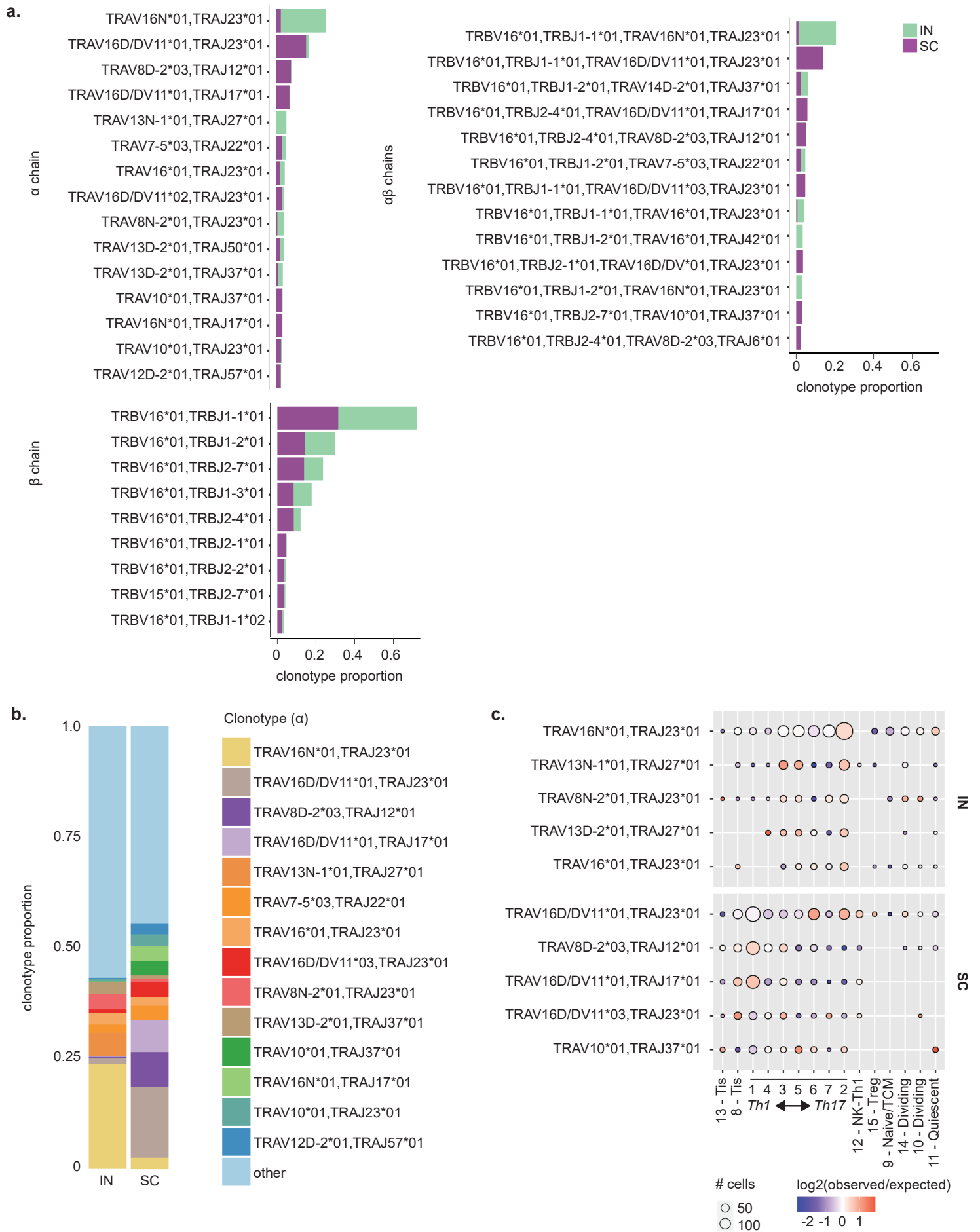


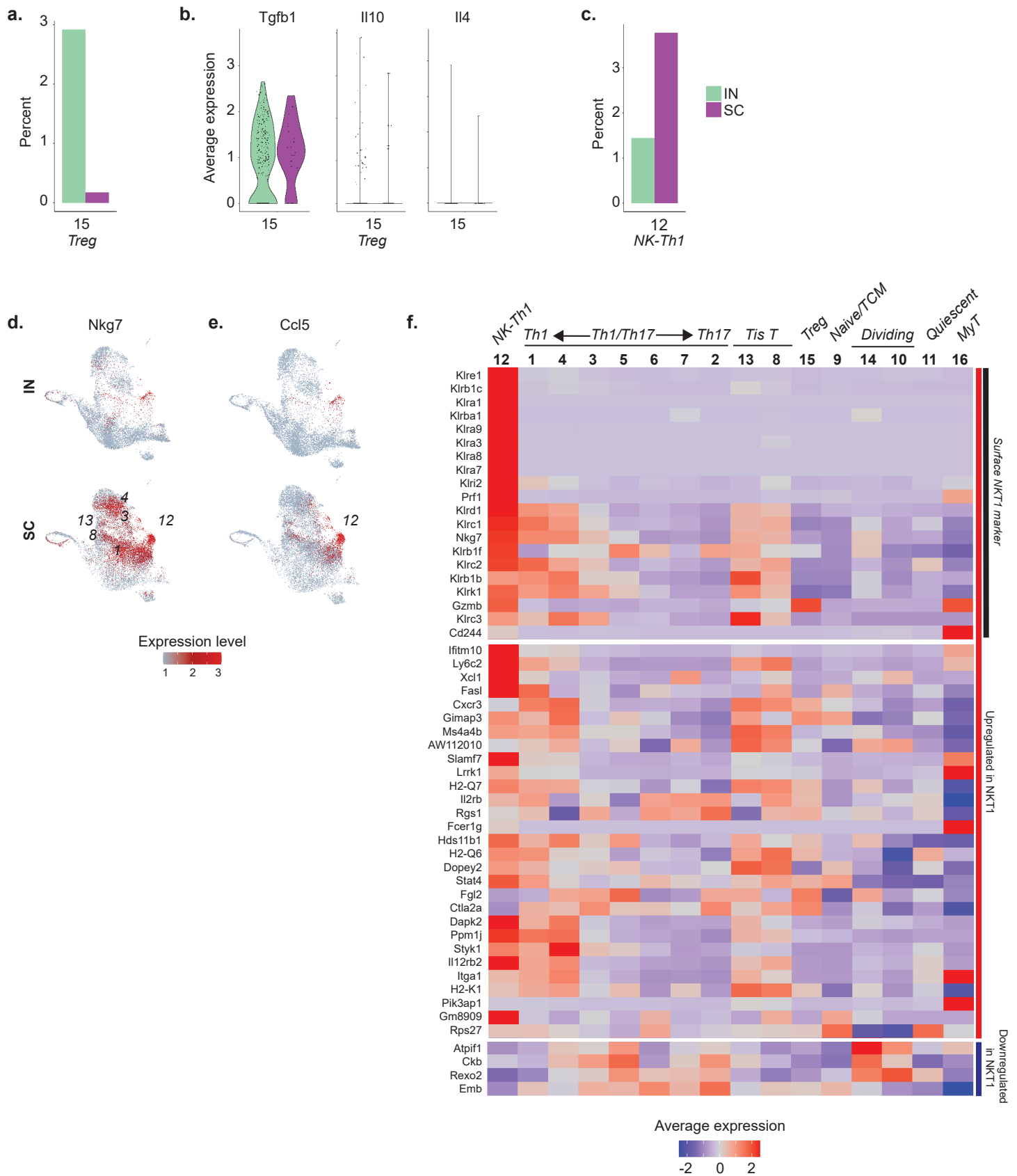
c.



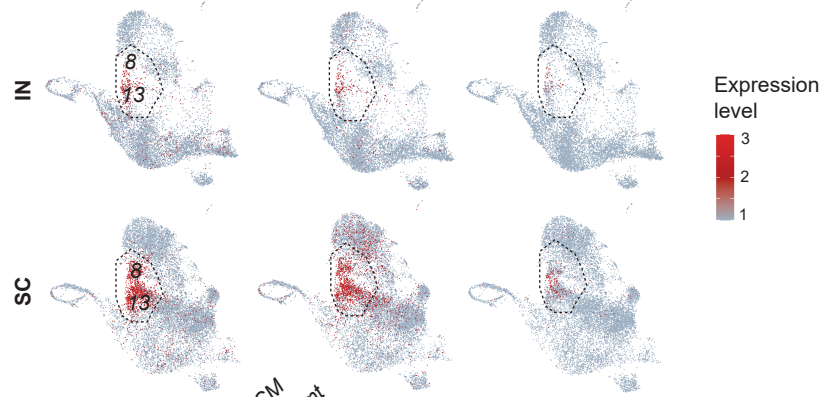
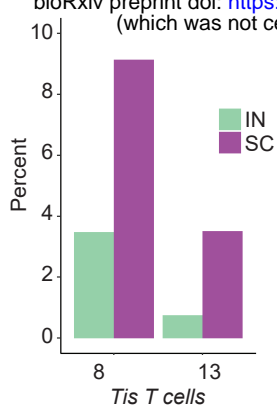




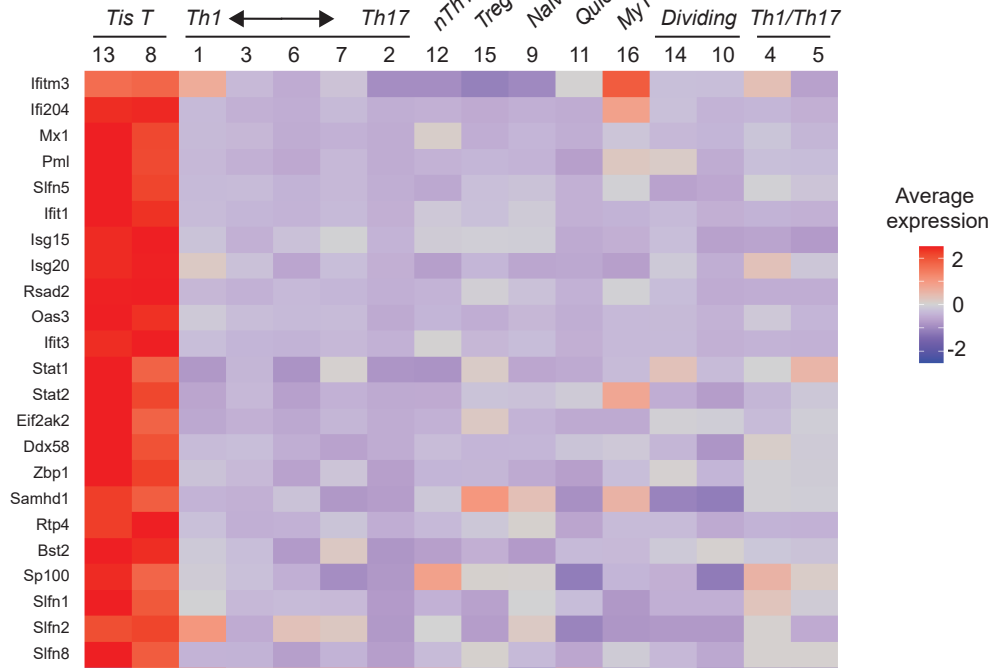




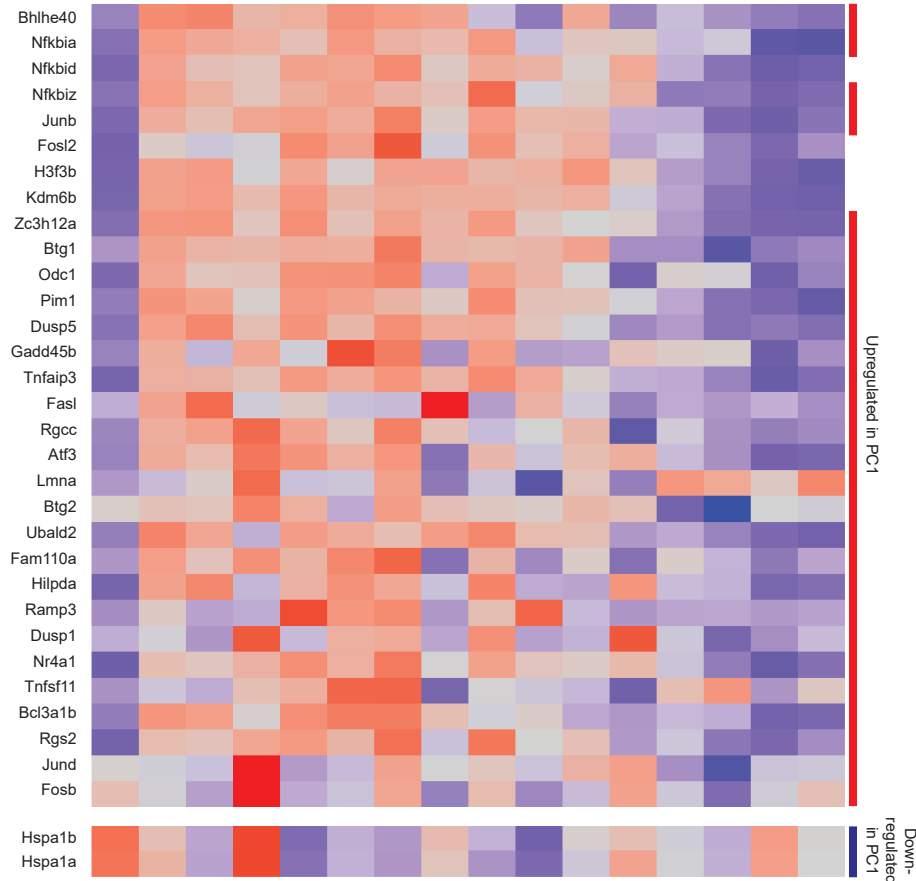
a.



c.



d.



e.

